"This paper develops a scanning strategy for the upcoming GeoCarb mission from geostationary orbit, using an optimization algorithm to establish the greatest return in terms of soundings that exceed an unspecified minimum threshold in signal-to-noise ratio (SNR). The development of the approach appears logical and seems to give reasonable results. To me, though, it feels like a starting point for a more detailed treatment. It treats the land masses of the Americas as a "uniform space," treating all points as equally important. While it is crucial to obtain global coverage (over the viewing area of the satellite), it seems to me that not all locations are equivalent in terms of monitoring greenhouse gas emissions. There are presumably hot spots of industrial activity that could benefit from closer scrutiny. The measurements do no extend to high enough latitude to capture emissions from the Alberta oil sands, but you will measure over the U.S. oil shale deposits in Colorado, Utah, and Wyoming, for example. I say this because one of the purported benefits of having the mission on a geostationary platform was that, according to the manuscript, "areas with high and uncertain anthropogenic emissions of CO2, CH4 and CO may be targeted with contiguous sampling," but this benefit is not exploited with the proposed scanning strategy. One would need to attribute increased weight to the hot spots to properly shade the coverage. The authors do mention the notion of adjusting the coverage to study events such as volcanoes and large wildfires, but that is a separate notion, a temporary campaign mode rather than a regular coverage strategy."

Our original goal for this study was to quantitatively obtain a scanning strategy that would cover the satellite viewing area once and result in the highest quality measurements of the Americas. The decision was made to scan the area between 50 degrees north and 50 degrees south in our study because it includes the areas of interest in the six science hypotheses stated in Moore et al (2018). To make this clearer to the reader, we've included the six hypotheses in the introduction.

We also agreed that demonstrating a scanning strategy with equal weighting for all land masses in the satellite viewing area does not illustrate to the reader the advantage of a geostationary platform. Therefore, we ran an additional experiment for a "city campaign" mode and added it to Section 5 of our manuscript. We would like to reiterate that this study is just a demonstration of one of many possible techniques and is not the proposed scanning strategy for the GeoCarb mission.

"Another benefit mentioned for the geostationary platform was that you could improve the signal by increasing the dwell time for a measurement. I do not know if there is some constraint that would require every scan to be identical. If one could select the measurement dwell time employed in each individual scan, for example, one could improve the results in regions where a large percentage of the soundings would otherwise fall below the SNR threshold and therefore be tagged as unusable. In this scenario, scan time would become an additional parameter to include in the optimization."

GeoCarb does not have the measurement dwell time as a parameter to be optimized since the long observation slit will, in general, cover areas of both low and high SNR in every scan. Additionally, maximizing observations from low SNR areas is not a primary goal of the mission, as seen in Moore et al (2018).

"The authors indicate that no results above the oceans are possible due to low signal. Is there no possibility of making use of ocean glint, as the OCO-2 mission does? This would obviously only work at certain times, when the conditions were such that sunlight reflected off the ocean at the same angle that the instrument was viewing the surface, but it would expand the coverage."

It is true that GeoCarb can theoretically make observations of ocean glint, but that is also not a primary objective of the mission.

"Judging from Figure 4, the gain in "usable soundings" relative to the baseline approach appears to be strongly related to a reduced number of measurements over the oceans. The expected improvement in errors over the Amazon is presumably related to the increased number of overlapping scans in that region."

In general, the increased number of overlapping scans is indeed a reason for increased number of soundings. However, we have added histogram plots of airmass and solar zenith angle, which are the stationary parameters on which our algorithm optimizes on, to show that the algorithm is selecting scanning blocks at peak airmass and solar zenith angle more than the baseline strategy.

"Note that no mention was made of what constituted a usable sounding. The last sentence relates the gain in soundings with SNR > 100, but it is not clear if that was the threshold employed for the determination of whether a particular measurement was usable. Based on the discussion on page 4, the calculated SNR was associated with the O2 A-band measurements. That means you assumed the SNR for the measurements of the CO2 bands was higher, or at the very least comparable?"

That was a typo and it has been corrected to say the SNR associated with the Weak CO2 band.

"In the text (page 8, lines 9-10), the statement is made that Figure 6 showed the minimum error distribution medians and variances occur where both weights are equal to 1. For me, that does not seem like an obvious conclusion to draw from the figure. It certainly seems true for the upper left panel, and maybe for the median in the upper right panel, but unless I misinterpret what is being said, I do not see it for the other plots."

We changed our language to say that the weighting of the terms does not have a large impact on the predicted error. We point that the spread of error medians and variances is approximately 0.01 ppm and ultimately decided to leave the weighting at 1.

"Minor comments
Page 2, line 2: the acronym "FoV" was defined but not used again, so there is no need to define the acronym"

Fixed in manuscript.

"Page 8, line 9: "Figure 6" should be "Fig. 6""

Since the figure is referenced at the beginning of the sentence, AMT guidelines tell us to spell out the entire word.

"Page 8, line 17: "Fig. 7 and 8" should probably be "Figs. 7 and 8""

Fixed in manuscript.

"Page 9, line 9: … mean Error… >Why is "Error" capitalized?"

Fixed in manuscript.

"Page 9, line 13: "Fig. 5 and 10" should probably be "Figs. 5 and 10""

Fixed in manuscript.

"Page 10, lines 4-5: "We also found that by optimizing for the global distribution of error, we obtained an improvement in regional errors as well, seen in Fig. 8" >This is not true for all regions, maybe an "overall improvement""

We agreed and fixed our language to state an "overall" improvement rather than the former.

"Page 10, line 13: the acronym "AOD" is not defined"

Now defined in manuscript.

"Figure 2: The caption claims that the plots relate to June (on the left) and December (on the right). The titles on the plots suggest they relate to September (on the left) and June (on the right)."

Fixed in manuscript.

"Figure 6: The variables w_dist and w_overlap are used to label the plots rather than w_d and w_o, the variables employed in the text."

Noted in caption.

"In Figures 8 and 9, it looks like there are no results over Cuba (greyed out?), even though that region appears to be within the scan range."

Cuba is not included in our scanning region as it is not a region of interest for the six hypotheses listed in Moore et al (2018).

"The manuscript deals with the optimization of geographic coverage, which is a problem of interest for geostationary satellite remote sensing. The approach presented in the manuscript is new and deserves publication in AMT. However, the approach and its underlying assumptions need to be better explained and the discussion of the results needs to be made clearer. The manuscript needs to be revised addressing the issues identified below.

1. The proposed scheme aims at enhancing the yield and quality of a geostationary CO2 observation system by optimizing the scanning strategy with a focus on the Signal to Noise Ratio (SNR). Many other parameters that are expected to drive the yield and quality of such observations are not taken into account. Degraded CO2 product quality is expected not only in cases with low SNR, but also in many other conditions e.g. when viewing geometries are slant, when target air masses contain clouds or aerosol, and when clouds cover parts of the field of view thus increasing the risk of spatial straylight. The choice of focusing on SNR needs to be justified, and the approach regarding other potential drivers need to be explained and motivated."

We do include slant geometry into our calculation of SNR. We acknowledge that cloud contamination can cause bias in our measurements, but quantifying that effect is an open research topic and beyond the scope of this paper. The long viewing slit of GeoCarb means that at any given time there is a high probability that part of the slit will be obscured by clouds. Therefore, adaptive scanning to avoid clouds is beyond the scope of this first demonstration. Our algorithm seeks to maximize SNR by looking at the drivers that are more stationary processes such as the airmass and surface reflectance.

"2. The link between radiometric noise and the total CO2 uncertainty need to be dis-cussed in more detail (beyond reference to O'Brian, 2016 and Eq. 3). The main contributors to the CO2 product uncertainty budget need to be discussed, and it needs to be explained why the optimization is driven by the random radiometric error."

The model we use is an empirical model of retrieval uncertainty as a function of SNR, not the actual physical models used in the L2 algorithm. We would like to point out that we are not minimizing total CO2 uncertainty, but rather uncertainty due to stationary processes such as the solar zenith angle, surface reflectance, and airmass. We have added additional explanation to Section 3.3 as to how we linked SNR to retrieved CO2 uncertainty.

"3. The objective function given (Eq. 5) minimized in the optimization scheme seems incomplete. The SNR depends on the radiance signal level (Eq. 2) hence also on the solar zenith angle (SZA) (Eq. 1). However, the SZA does not appear explicitly in the objective function. The penalty on slant illumination conditions seems to be missing."

The penalty for slant illumination is contained in the airmass factor, *m*. As a matter of fact, we initially had SZA explicitly in our objective function. However, the viewing slit of the GeoCarb instrument is so long that the slant penalty accounted over the entire area of a scanning block can outweigh other penalties such as overlapping coverage. This would cause the algorithm to pick too many overlapping blocks and extend the scan past the usable daytime. Therefore, we found that the SZA accounted by the airmass factor was sufficient.

"4. The top-level concept of the optimization scheme needs to be explained upfront (i.e. briefly in the abstract and in more detail in the introduction). Please clarify key elements such as a) that the scheme is to be applied off-line to determine a static scanning strategy, b) that near-real time information e.g. on cloud conditions is not taken into account, c) that the scheme is implemented by incrementally adding observation blocks, d) that the selection of the added blocks is performed by optimizing parameters X, Y, Z."

a) The technique demonstrated in the paper was indeed applied offline and it has been noted in the manuscript. We would like to point out that this IO routine could be applied online with real-time information.

b) The technique demonstrated in the paper assumes cloud-free atmosphere. This has been specified in sections 2, 3, 3.3, and 4. We know that this is physically incorrect and we believe that, in the future, the IO routine can be modified to take in real-time cloud information if it were available for the entire scanning region. Although as previously mentioned, that area of research is beyond the scope of this paper. We would like to reiterate that this is just a demonstration of a technique and not the proposed scanning strategy for the GeoCarb mission.

c), d) Additional explanation of the main idea of IO has been added to the abstract and introduction.

"5. It is concluded that the IO based solution outperforms the "obvious human" solution. This statement needs to be either better supported addressing a the apparent weaknesses listed below, or revised. Weaknesses include: a) the "obvious human"solution is to some degree arbitrary, there might be better guesses; b) comparisons are shown only for two cases with similar time of day, the situation can be different for other times; c) improvements in Amazonia and degradations at other places are reported (Fig 8), but it is not clear how global performances are determined and compared; d) differences in the total number of usable observations are reported (Section4.1) but the basis of these numbers is unclear; How is the number of 'usable soundings' determined? Are there thresholds on SZA, AMF, SNR, albedo, .. ?"

a) Prior to submitting this paper, the Moore et al (2018) had not been published. We possessed a tentative strategy and chose "obvious human" solution as a stand in for calling it the "proposed strategy" up until now. We have changed the language to say "proposed scanning strategy" rather than "obvious human" solution, referring to Moore et al (2018) as the source document for the GeoCarb mission description.

b) Part of the technique is that the algorithm chooses a timeframe for scanning by using a specified "starting airmass factor (AF) threshold" parameter. After specifying a starting AF threshold, the decision of when and where to start scanning is left to the algorithm. This is specified in Section 3.2.

c) Global performance in our context is meant to signify the aggregate predicted observational uncertainty (from Eq. (3) now Eq. (4)) over our satellite viewing area. We altered the language of the manuscript to clarify this.

d) We chose an SNR of 100 as our threshold as to what constitutes a usable sounding. In the empirical model of predicted CO2 retrieval uncertainty as a function of SNR, a SNR of 100 translates to a 2 ppm XCO2 retrieval uncertainty, which is within the first proposed accuracy per sample of XCO2 mentioned in Polonsky et al (2014). We have added extra explanation to the manuscript to clarify this.

"6. Section 4.2 reports a sensitivity analysis based on the assessment of regression coefficients. The conclusion of this analysis is unclear. Please clarify the conclusion in Section 4.2 and discuss the result in the overall context, in Section 5.7. Figures 5 and 10 are not understood. Specify, also in the caption, which parameter is plotted on the ordinate, what the colour coding means, which distributions are represented by the 'violins'. Why are distributions plotted as double-sided graphs?"

The x-axes of Figs. 5 and 10 are labeled as "starting threshold" in reference to the starting airmass factor threshold that the algorithm takes as a parameter. The colors are not in reference to any specific attribute of the distribution, rather it just makes it easier to distinguish between different distributions. We chose to represent our distributions as violins because we felt that it makes it easy for the reader to identify areas of high density within each distribution.

The sensitivity analysis was performed post-simulation runs as a check to see if the algorithm would exhibit unexpected behaviors when perturbed and concluded that it does not. These results are not tied to the main results of this paper. Therefore, the sensitivity analysis was moved to the appendix.

"Technical Corrections
Section 3.6 The iterative determination of scanning blocks might be dependent on the starting point (the location of the first scanning block). Have various different starting positions been investigated?"

As mentioned in response to comment 5, the algorithm takes a specified starting airmass factor threshold as an argument and then it decides when and where to start scanning. As a pseudo-sensitivity check early in conducting our experiments, we did try to force the algorithm to start at different areas, but it would return to scanning generally the same geographic locations as other algorithm-selected strategies within a short time after starting the scan.

"Section 3.5.2 Is full and contiguous coverage of the continental Americas within +/- 50deg lat within a day a hard boundary conditions for the optimization?"

Yes. We have added additional explanation to the background section that explains that this geographic region includes the regions of interest for the six major science hypotheses stated in Moore et al (2018).

"Page 4 line 18: the aerosol optical thickness of 0.3 is considered very large. Please justify. Aerosol optical depth depends on wavelength. What is the reference wavelength for the optical depth values provided?"

We chose an aerosol optical thickness of 0.3 because it is considered a worst-case scenario for clear-sky retrievals and would give us conservative estimates of predicted observational uncertainty. This decision was based on the experience of the ACOS and OCO-2 team, referenced in the manuscript. We have added additional language clarifying that we are looking at the weak CO2 (1.61 micron) band.

"Page 4 Eq 2: please provide units of parameters N0 and N1 (which should be sameas the units of I)"

Units have been added clarifying that *I*, *N0* and *N1* are in units of $nW\ (cm^2\ sr\ cm^{-1})^{-1}$

"Page 4 Eq 3: please clarify the meaning of sigma (introduced as the observational uncertainty). Clarify whether it is taken as the dominant contribution to the XCO2vertical column uncertainty. Discuss the validity of this assumption."

Additional explanation of sigma was added to Section 3.3, which explains that sigma is derived from the posterior covariance given by the L2 algorithm.

"Page 4 Eq 3: Specify units of sigma."

The manuscript has been fixed to say that sigma is in units of ppm.

"Page 5 Eq 4: eq 2 established a simple noise model. Eq 5 established an alternative more simplistic noise model. Why is the latter needed?"

The more simplified model in Eq. 5 is an intermediate step to explaining the formulations of the objective function. It has been moved to be an inline equation rather than a numbered equation block.

"Page 5 line 7: unclear what is meant with "multiplicative inverse""

Additional language was added to clarify that we mean, one divided by the radiance.

"Page 5 Eq 5: 's' is used in an inconsistent way. It is introduced as an index to label the candidate block. It appears as a parameter in the argument AF, where it probably should not appear since x and y already capture the horizontal spatial dimensions. At the same time it represents an area in the spatial overlap operation; instead a dedicated variable (eg A_s) should be used to represent the area of the candidate block s."

We realized that having set operations in the equation could be ambiguous to the reader. The terms in the objective function were reformulated to exclude set operations.

"Page 5 Eq 5: specify across which domain the median is evaluated. I guess it is the area of the candidate block 's'."

Additional language was added to clarify that we meant the area of the candidate block, s.

"Page 5 Eq 5: The variables E and I should be introduced as 'areas of' the target landmass and of the selected scan blocks."

The terms in the objective function were reformulated to be more clear to the reader.

"Page 5 Eq 5: the distance delta is not well defined. Please clarify from which point to which point is it to be evaluated."

Additional language was added to clarify that delta is the shortest linear distance from the boundary of the last selected scan block to the candidate scan block. A diagram has also been added to clarify the terms of distance, overlap, and coverage.

"Page 6 Section 3.5 discusses a finite number of possible locations of a scan block, which suggests that blocks can be located only at discrete positions. Please clarify whether this is correct. If so, introduce this constraint explicitly and specify the grid of candidate locations."

Additional explanation was added to Section 3.5, referencing the explanation of the formulation of scan blocks in Section 3.1.

"Section 3.5 Page 6 Section 3.5 line 9-10: The formulation "...a Greedy heuristic algorithm was employed to find a minimal covering set as a lower-bound estimate for set cardinality " is not understood. Please clarify what is meant with the term 'cardinality' in the present context?"

The term 'cardinality' has been changed to say "set size".

"Page 7 line 7-10 very long sentence, meaning is unclear. Please split and reformulate.
Page 7 line 7-10 The variance of predicted errors is mentioned. On which parameter and over which domain is this variance evaluated?"

We believe that the commenter is referencing to Page 8 lines 7-10. The entire Section 3.7 (now Sect. 3.6) has been reformulated for clarity.

"Page 7 line 7-10 Please clarify and elaborate how to the optimum at weights=1 is found."

We changed our language to say that the weighting of the terms have negligible effects on the predicted error. We point that the spread of error medians and variances is approximately 0.01 ppm and ultimately decided that the weights shall remain equal to 1.

The following is the marked up manuscript. The language added to the original manuscript is highlighted in **blue**. The language removed from the original manuscript is striked out in ~~**red**~~.

An SNR-Optimized Scanning Strategy for the Geostationary Carbon Cycle Observatory (GeoCarb) Instrument

Jeffrey Nivitanont[1], Sean M. R. Crowell[2], and Berrien Moore III[2]

[1]Department of Mathematics, University of Oklahoma, Norman, OK, USA
[2]College of Atmospheric and Geographic Sciences, University of Oklahoma, Norman, OK, USA

Correspondence: Jeffrey Nivitanont (jeffniv@ou.edu)

Abstract. The Geostationary Carbon Cycle Observatory (GeoCarb) will make measurements of greenhouse gases over the ~~land mass in the western hemisphere~~contiguous North and South American land masses at daily temporal resolution. The extreme flexibility of observing from geostationary orbit induces an optimization problem, as operators must choose what to observe and when. The proposed scanning strategy for the GeoCarb mission tracks the sun's path from East to West and covers the entire area of interest in five coherent regions in the order of Tropical South America East, Tropical South America West, Temperate South America, Tropical North America, and Temperate North America. We express this problem in terms of ~~an optimal subcovering~~ a geometric set cover problem, and use an ~~Incremental Optimization~~ incremental optimization (IO) algorithm to create a scanning strategy that minimizes expected error as a function of the signal-to-noise ratio (SNR)~~, and show that this method outperforms the "human selected" strategy in terms of global error distributions~~.

The IO algorithm used in this studied is a modified Greedy algorithm that selects, incrementally at 5-minute intervals, the scanning areas with the highest predicted SNR with respect to airmass factor (AF) and solar zenith angle (SZA) while also considering operational constraints to minimize overlapping scans and observations over water. As a proof of concept, two experiments are performed applying offline the IO algorithm to create an SNR-optimized strategy and compare it to the proposed strategy. The first experiment considers all land masses with equal importance and the second experiment illustrates a temporary campaign mode that gives major urban areas greater importance weighting. Using a simple instrument model, we found that there is a significant performance increase with respect to overall predicted error when comparing the algorithm-selected scanning strategies to the proposed scanning strategy.

1 Introduction

Understanding the effects of anthropogenic carbon dioxide (CO_2) on the carbon cycle requires us to understand the spatial distribution of atmospheric CO_2 concentrations to identify natural and anthropogenic sources and sinks. In addition to a sparse in situ sampling network, ground-based remote sensing measurements are currently obtained from the Total Column Carbon Observing Network (TCCON) and space-based measurements from the Orbiting Carbon Observatory (OCO-2) (Eldering et al. (2017a), Eldering et al. (2017b), Crisp et al. (2017), Crisp et al. (2008), Crisp et al. (2004)) and Greenhouse Gases Observing Satellite (GOSAT) (Kuze et al. (2009), Yokota et al. (2009), Hammerling et al. (2012)). These instruments have provided a

wealth of data for understanding the global carbon cycle in ~~the~~ recent years. However, these instruments have spatial and temporal limitations. The repeat cycles of the space-based instruments force the spatial and temporal interpolation of the atmospheric CO_2 concentrations within their respective cycles, 3 days for GOSAT (Kuze et al. (2009)) and 16 days for OCO-2 (Miller et al. (2007)). The sparsity of the TCCON measurement sites restricts the latitudinal range of observations. The new Geostationary Carbon Cycle Observatory (GeoCarb) (Moore et al. (2018), Polonsky et al. (2014)) will ~~allow us to~~ provide measurements that augment the current remote sensors on the ground and in space in both temporal and spatial coverage.

Recently selected as ~~the~~ NASA's Earth Venture Mission-2 (EVM-2), GeoCarb is set to launch into geostationary orbit in 2022 to be positioned at ~~$85°W$~~ approximately 85° (±15°) West longitude, with the mission of improving the understanding of the carbon cycle. Building on the work of OCO-2, GeoCarb will observe reflected sunlight daily over the Americas, and retrieve the column average dry air mole fraction of carbon dioxide (XCO_2), carbon monoxide (XCO), methane (XCH_4), and solar-induced fluorescence (SIF). ~~GeoCarb views~~ Moore et al. (2018) identify six major hypotheses about the Carbon-Climate connnection that the GeoCarb mission aims to provide insight on: (1) The ratio of the CO_2 fossil source to biotic sink the conterminous United States (CONUS) is ~4:1, (2) Variation in productivity controls the spatial pattern of terrestrial uptake of CO_2, (3) The Amazonian Forest is a significant (0.5–1.0 PgC/year) net terrestrial sink for CO_2, (4) Tropical Amazonian ecosystems are a large (50–100 PgC/year) source for CH_4, (5) The CONUS methane emissions are a factor 1.6 ± 0.3 larger than in the EPA database, (6) Larger cities are more CO2 emissions efficient than smaller ones. These six hypothesis were used as a basis to select the ~85°W observing slot as the position with most "potential for significant scientific advances."

GeoCarb will view reflected sunlight from Earth through a narrow slit that projects on the Earth's surface to an area measuring about 1,~~740~~ 690 miles (2,~~800~~ 700 kilometers) from north to south and about ~~3.7 miles (6~~ 3.2 miles (5.2 kilometers) from east to west. The instrument ~~makes~~ will make measurements along the slit with a ~~4.5 second integration~~ ~9 second integration time. Instrument pointing ~~is~~ will be accomplished by way of two scanning mirrors that shift the field of view ~~(FoV)~~ north-south and east-west. The pointing system is extremely flexible, and observations can be made at any location ~~at any~~ and time with sufficient solar illumination. This flexibility induces an optimization problem: ~~where~~ Where should the instrument take measurements at a given time throughout the day?

Determining when and where to make daily scans with GeoCarb's observing capabilities is mathematically similar to a CO_2 ground observation network optimization problem for establishing new observation sites. Selecting the optimal location of new observing stations has been shown to be feasible by utilizing various optimization algorithms. There have been previous studies performed on the problem of optimizing CO_2 observation networks utilizing computationally expensive evolutionary algorithms [i.e., Simulated Annealing (Rayner et al. (1996); Gloor et al. (2000)) and Genetic Algorithm (Nickless et al. (2018))] and one utilizing a deterministic, incremental optimization (IO) algorithm (Patra and Maksyutov (2002)). All of the previous studies ~~utilized~~ mentioned employed their optimization routines to minimize CO_2 measurement uncertainty as a function of signal-to-noise ratio (SNR).

In this paper, a deterministic, ~~incremental optimization routine (IO)~~ IO routine is utilized to find a ~~scanning strategy for GeoCarb that minimizes expected~~ geostationary scanning strategy that minimizes GeoCarb's expected CO_2 measurement uncertainty as a function of SNR ~~. Section 2~~ for the satellite viewing area. Section 2 gives background information on the GeoCarb

mission and the objectives for this paper. Section ~~3~~ 3 explains the process used to create the ~~SNR-optimized~~ SNR-optimizing, IO algorithm and how the expected error is calculated from the simulated retrievals. In Section ~~4, the distribution of global error of the~~ 4, a comparison is done between an algorithm-selected strategy ~~is compared to a baseline strategy to determine the performance of the algorithm and the sensitivity of algorithmto inputs is investigated, with results discussed in Sect. 5.~~ and the baseline strategy in the case where all American land masses between 50°N and 50°S are scanned with equal importance weighting. In Section 5, a case study is performed to exhibit a "city campaign" mode for the IO algorithm. We offer concluding statements in Sect. ~~6~~ 6 and future research goals.

2 Background

GeoCarb will be hosted on a SES Government Solutions (http://www.ses-gs.com) communications satellite in geostationary orbit at ~~85°~~ ~ 85°W. It will measure reflected ~~near-infrared~~ sunlight in the O_2 band at 0.76μm to measure total column O_2, the weak and strong CO_2 bands at 1.61μm and 2.06μm to measure XCO_2, and the CH_4 ~~and CO bands~~ band at 2.32μm for measuring XCH_4 and XCO. The O_2 spectral band ~~is identical to that of the OCO-2 mission and~~ allows for determination of mixing ratios and the measurement of SIF, as well as additional information on aerosol and cloud contamination of retrievals. The baseline mission for GeoCarb aims to produce column-averaged mixing ratios of ~~CO2, CH4~~ CO_2, CH_4 and CO with accuracy per sample of 0.7% (≈ 2.7 ppm), 1% (≈ 18 ppb), and 10% (≈ 10 ppb), respectively (Polonsky et al. (2014)). Geostationary orbit offers two main advantages over low Earth orbit (LEO). First, the signal-to-noise ratio (SNR) is proportional to the square root of the dwell time for detectors limited by photon shot noise~~. Geostationary~~ , and geostationary orbits enables longer observation times, thereby increasing SNR. Second, due to the flexibility of the scanning mirrors, areas with high and uncertain anthropogenic emissions of CO_2, CH_4 and CO may be targeted with contiguous sampling, relatively small spatial footprints, and fine temporal resolution allowing for several observations per day on continental scales~~are possible~~.

We are presented with the problem of finding an optimized scanning strategy for the GeoCarb satellite instrument. The underlying abstract mathematical problem related to optimizing the scanning pattern is the ~~Geometric Set Cover~~ geometric set cover problem (Hetland (2014)). Given a finite set of points in space and a ~~set of subsets~~ collection of subsets of those points, the objective is to find a minimal set of ~~scan blocks~~ subsets whose union covers all the points in the space. ~~This idea is identical to a network optimization problemcomparing the coverage area of a potential network observation site to a geometric subset in the space to be covered.~~ The classical method for finding a solution to the geometric set cover problem is to employ a Greedy algorithm. Greedy algorithms incrementally choose optimal solutions based on the available information at a given time. In the context of the geometric set cover problem, the Greedy algorithm incrementally selects subsets that cover the most amount of uncovered points until all points are covered by the chosen subsets. Modifying the Greedy algorithm to optimize an objective function at each iteration is a common routine for finding geometric solutions to spatial problems with no known analytical solutions.

The task of determining the locations of new observation sites so that the total number of required sites to cover an area is minimal ~~is solved similarly. Therefore, we looked at methods used for optimizing network observation sites for our~~

application. However, our motivation extends beyond just finding a minimal covering setthas been solved using IO algorithms (Rayner et al. (1996); Gloor et al. (2000); Patra and Maksyutov (2002)). Finding an optimized scanning strategy for GeoCarb is identical to an observation network optimization problem. Therefore, these IO algorithms were prospective candidates for application to GeoCarb. Our goal is was to find a minimal covering set that translates to a scanning strategy that is operationally efficient and minimizes global measurement error for the GeoCarb instrument.

Specific to the instrument

3 Methods

Translating the idea of the geometric set cover problem to GeoCarb's application, the collection of geometric subsets are 5-minute East-to-West scan blocks, shown in Fig. 1, and the . The points in space that we are trying to cover is to be covered are the North American and South American land masses between $50°N$ and $50°S$. Because measurement since this contains the regions relevant to the six science hypotheses mentioned in the introduction. Measurement errors are influenced by parameters that vary in space and time such as clouds, airmass, and solar zenith angle. Predicting cloud formation and quantifying the effects of clouds on measurement errors are active areas of research. For simplicity and computational efficiency, a cloud-free atmosphere is assumed in the simple instrument model. Surface albedo is assumed to be constant within the span of a day. Due to time-dependency, the solutions are in the form of ordered sets where the scan blocks are ordered by time of execution. These solutions are referred to in this paper as scanning strategies. With the simplifying assumptions of making our making the problem computationally tractable and minimizing scan coverage over the ocean, we propose a candidate set of 135 scan blocks (is proposed in Fig. 1). This is a much larger candidate set than those of the network optimization studies that utilized evolutionary algorithms (Rayner et al. (1996); Gloor et al. (2000)). Therefore, the computationally efficient Incremental Optimization (IO) procedure IO algorithm, which is a modified Greedy algorithm, was implemented to select scan blocks that minimize our objective function at each increment in time.

4 Methods

3.1 Scan Blocks

We assume The scanning region is discretized in the east-west direction assuming that GeoCarb will process commands in terms of 5-minute scan blocks, during which the instrument steps . During the scan the instrument will step the slit from east to west . The set of considered scan blocks , shown in Fig. 1, purposely excludes potential within the scan block. Each slit observation is proposed to contain approximately 1000 individual soundings and is assumed to have a ~ 9 second integration time. The scanning region is further discretized in the north-south direction by scan blocks separated by $5°$ latitude increments. Potential scans that are primarily over the ocean , as GeoCarb will not be able to make retrievals over water surfaces due to lack of signal in the CO_2 spectral bands. The potential scans are also largely are excluded, since measurements over the ocean are not a priority for the GeoCarb mission. The scan blocks are also restricted to land between $50°N$ and below $50°S$ as a hard

constraint due to larger ~~solar~~ sensor viewing zenith angles at the higher latitudes~~. Each slit observation (i.e. 1016 individual soundings) is assumed to take 5 seconds, after which the slit moves to the west by half a slit width~~, though this area still includes all regions relevant to the six science hypotheses mentioned in the introduction. The resulting set of candidate scan blocks are shown in Fig. 1.

3.2 Science Operations Timeline

A goal of this study is to create a scanning strategy that views all land masses of interest at least once within the time window of usable daylight. To determine what time of day to begin the scanning process, Macapá, Brazil and Mexico City, Mexico were chosen as geographic reference points to determine the beginning and ending time, respectively, of the usable daylight time frame. Macapá is located at $(0°, 50°W)$ at the mouth of the Amazon river and being on the equator gives us a consistent starting time relative to airmass factor (AF), a function of solar zenith angle (SZA) and the sensor viewing zenith angle (~~ZA~~VZA), where AF $= \frac{1}{\cos(\text{SZA})} + \frac{1}{\cos(\text{ZA})} = \frac{1}{\cos(\text{SZA})} + \frac{1}{\cos(\text{VZA})}$. Located at $(19.5°N, 99.25°W)$, Mexico City, Mexico is an ideal reference point to determine when the window of usable daylight ended because it is longitudinally centered in the North American land mass while being close enough to the equator for the calculated airmass factors to remain consistent through the winter months. The ~~scanning strategy~~ IO algorithm calculates the starting time when Macapá first exceeds a starting threshold for AF and the ending time when Mexico City drops below an ending threshold for AF to determine when the usable daylight time window is over. As a result of parameter exploration experiments described in ~~section 3.7~~Sect. 3.7 , the suggested starting threshold is AF $= 2.6$ for the Summer Solstice and AF $= 2.7$ for the Autumn Equinox for minimum variance in predicted errors.

3.3 Uncertainty in Retrieved Gas Concentrations

~~GeoCarb retrieves gas concentrations using reflected sunlight. The radiance, I,~~ Errors in retrieved gases are a result of numerous different sources, including imperfect radiometric calibration, errors in differential absorption spectroscopy, variations in the instrument line shape, and others. For simplicity, we assume that the errors in retrieved gases are arise from instrument noise as specified by a simple noise model arising from GeoCarb specific design parameters. The signal to noise ratio is then propagated through to uncertainty using a simple parameterization that was trained on retrieval results from simulated data.

The radiance observed by GeoCarb is an aggregate of insolation and atmospheric and land surface processes that absorb, reflect, and scatter photons. The impact of these processes is parameterized using a simple model, I, from Polonsky et al. (2014) that incorporates the effects of surface albedo and attenuation by aerosols over the sun-Earth-satellite path described by ~~the solar zenith angle (SZA) and the sensor zenith angle (ZA):~~ SZA and VZA:

$$I = \mathrm{F_{sun}} \alpha \cos(\mathrm{SZA}) e^{-\mathrm{AF}\tau} \quad \mathrm{nW(cm^2\ sr\ cm^{-1})^{-1}} \tag{1}$$

where $\mathrm{F_{sun}}$ is the band-specific solar irradiance, α is the band-specific surface albedo, and τ is the optical depth (OD) of atmospheric scatterers (e.g. ~~aerosols). For our simple model, we assumed a~~ , aerosols, water). A cloud-free atmosphere is assumed for this simple model, whereas in the operational environment, clouds play a major role in retrieval quality due to

poorly understood 3-D scattering effects. As can be readily verified, larger zenith angles lead to reduced signal for constant scatterer OD, as does smaller surface albedo. Note that τ is a quantity with significant spatial and temporal variability, as aerosol concentrations are modified by atmospheric dynamics, emissions, and chemistry. Typical values of τ in successful retrievals for OCO-2 are less than 0.6 for nadir soundings near the equator and decrease as AF increases. Similarly, surface albedo varies with land cover type on small spatial scales, and throughout the year with vegetation density. The OD term was set to $\tau = 0.3$ as it was previously found to be a reasonable estimate for a "clear" sky retrieval (Crisp et al. (2004), O'Dell et al. (2012)).

An important indicator of observation quality is the signal-to-noise ratio (SNR). In the case of GeoCarb, the signal is ~~referred to as~~modeled as, I, and the instrument noise equivalent spectral radiance model, N, as

$$N(I) = \sqrt{{N_0}^2 + N_1 I} \quad \text{nW(cm}^2\text{ sr cm}^{-1})^{-1} \tag{2}$$

where N_0 and N_1 (in units nW(cm^2 sr cm^{-1})$^{-1}$) are parameters that empirically capture the effects of the instrument design (e.g., telescope length, detector noise) on overall instrument noise (O'Dell et al. (2012)). The ~~O~~Weak CO_2 ~~A-band (0.763~~band (1.61μm) specific constants ~~, $N_0 = 0.1819$ and $N_1 = 0.003295$~~ that represent a signal-independent noise floor radiance, $N_0 = 0.1296$, and shot noise due to observed signal radiance, $N_1 = 0.00175$ are used in ~~the noise model, which are~~ Eq. 2 to later calculate SNR. N_0 and N_1 are updated figures derived from the airborne trials with the Tropospheric Infrared Mapping Spectrometers (TIMS) by Lockheed Martin (Kumer et al. (2013)), ~~that were~~ and later revised in Polonsky et al. (2014). The SNR is then defined as $\frac{I}{N}$.

In O'Brien et al. (2016), the authors fitted an empirical model to predict the ~~observational uncertainty~~ posterior errors, σ, estimated by the L2 retrieval algorithm as a function of the measurement SNR. ~~They~~ In their case, σ was derived from the L2 retrieval algorithm posterior covariance given by

$$\hat{S} = (K^t S_\epsilon^{-1} K + S_a^{-1})^{-1} \tag{3}$$

where S_ϵ is the covariance of the instrument noise, S_a is the covariance of the distribution about the prior state, and K is the Jacobian of the transformation from states to measurements. This uncertainty represents the impacts of the noise on the fitted spectra as well as nonlinearities in the radiative transfer model. It does not account for systematic errors that account from model deficiencies or instrument mis-characterization, which are beyond the scope of this work. O'Brien et al. (2016) found that the ~~function~~

$$\sigma = \frac{1}{\frac{1}{14} + (0.0039)SNR}.$$

~~best captures the observation error distribution as SNR increases.~~ solid curves that best fit the posterior errors in the Weak CO_2 band were of the form $\sigma = \frac{a}{1+bx^c}$, where x is the SNR and a, b, c are real constants. For CO_2, σ represents uncertainty in ppm. For a SNR of $x = 0$, the function takes its maximum value of a. Therefore, a represents the prior uncertainty. With large values of x, the constant c determines the rate of decay for σ. Setting $a = 14$ ppm to express a conservative prior uncertainty

on retrieved CO_2 and $c = 1$, the resulting empirical model was

$$\sigma = \frac{14}{1 + (0.0546)x} \text{ppm}. \tag{4}$$

The same model is used to connect SNR and uncertainty for ~~later scanning strategy distributions. The~~ evaluating scanning strategies later in this paper. For the purpose of our experiments, the distribution of σ is treated as the metric against which a particular scanning sequence is evaluated.

3.4 Objective Function

Examining the definition of SNR, it is easy to see that

$$SNR = \frac{I}{N} \approx k\sqrt{I}, \text{ where } k \text{ is a constant.}$$

~~Since the goal is to ultimately maximize~~ $SNR \approx k\sqrt{I}$, where k is a constant. Therefore it is sufficient to focus on maximizing I~~, we define~~ . Maximizing I is equivalent to minimizing its multiplicative inverse, $\frac{1}{I}$. Therefore, an objective function ~~that minimizes its multiplicative inverse~~was defined that is approximately proportional to $\frac{1}{I}$ on the parameters AF and surface albedo. In addition to minimizing SNR, two constraints were included in the objective function to prevent erratic ~~behavior in the scanning strategy~~scanning behavior. An overlap term, ϕ, was introduced to minimize repeated coverage of regions. A distance term, δ, was also included ~~, which is the squared~~ to prevent erratic scanning behavior. δ is the shortest linear distance from the boundary of the last selected scan block to a candidate scan block. The objective function, c, to be minimized is given by

$$\text{c}(s,t) = \text{median}(e^{AF(s,t,x,y)}\alpha(x,y)^{-1})\psi(1 + \frac{(s \cap \mathbb{I}) + \delta^2}{s \cap \mathbb{E}} \frac{\phi + \delta^2}{\beta}), \tag{5}$$

where

$s =$ ~~A candidate~~ Candidate scan block.

$t =$ Time.

~~$\mathbb{E} =$ Uncovered land mass~~ $\beta =$ Area of uncovered land mass covered by the candidate scan block

~~$\mathbb{I} =$ The set of selected scan~~ $\phi =$ Area of overlapping coverage with selected blocks

~~$\alpha(x,y) =$ Surface albedo of a point in scan block.~~$\delta =$ ~~Distance from last selected scan block .~~$\psi =$ Median of $e^{AF}\alpha^{-1}$ over the entire area of the candidate scan block

~~$AF(s,t,x,y) =$ Airmass factor~~ $\alpha =$ The surface albedo of a point ~~in~~ within a scan block~~with respect to time.~~ .

The ~~median of $e^{AF(s,t,x,y)}\alpha(x,y)^{-1}$~~ terms ϕ, β, and δ are illustrated in Fig. 2 for clarity. The median of $e^{AF}\alpha^{-1}$ is used because ~~we assume~~ it is assumed that the distributions of airmass factor and surface albedo are non-Gaussian within the scan blocks due to the long viewing slit. The high variability of both parameters are described in Section ~~3.4.2~~ 3.4.2.

3.4.1 Surface Albedo

The MCD43C3 Version 6 White Sky Albedo MODIS band 6 data set (Schaaf and Wang (2015)) was utilized for obtaining surface albedo, α. The MODIS BRDF/Albedo product combines multiband, atmospherically corrected surface reflectance data from the MODIS and MISR instruments to fit a Bidirectional Reflectance Distribution Function (BRDF) in seven spectral bands at a 1 km spatial resolution on a 16-day cycle (Lucht et al. (2000)). The White Sky Albedo measure is a bihemispherical reflectance obtained by integrating the BRDF over all viewing and irradiance directions. These albedo measures are purely properties of the surface, therefore they are compatible with any atmospheric specification to provide true surface albedo as an input to regional and global climate models. The native data was aggregated to the $0.5°$ spatial resolution, and interpolated in time to daily resolution.

3.4.2 Seasonal Variation of Parameters

Since AF is affected by the sun's position and albedo is affected by the density of vegetation, there are large seasonal variations in both of these variables, shown in ~~Fig~~Figs. 3 and 4. However, there is little to no variation between day-to-day comparisons of these variables. It suffices then, and gives an added advantage of being computationally efficient, to calculate separate scanning strategies for each month rather than day.

3.5 Optimization Algorithms

The time-dependency of the scanning strategy requires the solutions to be represented as ordered scan blocks of the ~~candidate set~~discretized candidate set described in Sect. 3.1 and shown in Fig. 1. Therefore, the sum of permutations $\sum_{k=1}^{135} \frac{135!}{(135-k)!}$ gives approximately 7×10^{230} possible solutions. Since it is computationally intractable to evaluate all possible solutions, a Greedy heuristic algorithm was employed to find a minimal covering set as a lower-bound estimate for ~~set cardinality, and then it was~~ the size of a solution set. The Greedy algorithm was then modified to an ~~Incremental Optimization~~ incremental optimization (IO) algorithm to find a scanning strategy optimizing for SNR.

3.5.1 Greedy Algorithm

Viewing the North American and South American land masses as a uniform space to be covered without considering any additional constraints, the problem is a ~~Geometric Set Cover~~ geometric set cover problem where the goal is to find a minimal ~~cardinality~~ size covering set that we will call optimal. It is well-known that there are no known analytical solutions to the ~~Set Cover~~ set cover problem, as it is one of Karp's 21 NP-Complete problems, and the optimization version is NP-Hard (Karp (1972)). However, there exists a heuristic method for finding a solution called the Greedy algorithm that selects the cover with the largest intersection with the uncovered space recursively until the space is covered (Hetland (2014)). The pseudo-code of the Greedy routine is shown in Algorithm 1. The Greedy algorithm is computationally efficient, ~~though~~ but it is difficult to verify that the solution it finds is the ~~*optimal*~~ optimal solution. The Greedy algorithm is suitable for ~~our application~~ the purpose of finding the smallest size scanning strategy because it reduces the set of candidate blocks at each iteration by removing the

selected scan blocks ~~and this ensures~~ to ensure that there are no repeated scan blocks in a ~~scanning strategy~~solution. Running the Greedy heuristic with no objective function shows that the area of interest can be covered using 83 scan blocks. Therefore, ~~we took this~~ this was taken as the lower bound of covering set size.

Algorithm 1 Greedy Algorithm

$\mathbf{E} \leftarrow$ Space to be covered
$\mathbf{S} \leftarrow$ Set of scan blocks where $E \subseteq \bigcup s_i \in \mathbf{S}$
$\mathbf{I} \leftarrow \emptyset$
while $\mathbf{E} \subsetneq \mathbf{I}$ **do**
  Find $s^* \in \mathbf{S}$ such that $s^* \cap \mathbf{E}$ is maximal for all $s_i \in \mathbf{S}$
  Append s^* to $\mathbf{I}$
  Remove s^* from $\mathbf{S}$
end while

3.5.2 Incremental Optimization

The Greedy algorithm was modified to select the scan block that minimizes the objective function at each iteration to satisfy operational constraints. Presented in Patra and Maksyutov (2002), this modification to the Greedy algorithm ~~makes it an Incremental Optimization~~ is called an incremental optimization (IO) algorithm because its goal is to minimize the objective function at each increment of time to find the global optimum. Like the Greedy algorithm, IO has the advantage of being computationally inexpensive. However, it may find local optima only and produce sub-optimal solutions depending on the nature of the problem. Usually to avoid this issue, ~~it is common to introduce small perturbations~~ small perturbations are introduced at each increment, such as is done in evolutionary algorithms (~~i.e.~~e.g., simulated annealing and genetic algorithm). It has been shown that IO yields results that are nearly as good as evolutionary algorithms while using a fraction of the computational power (Nickless et al. (2018)).

For GeoCarb's application, we were looking at the global distribution of errors, σ, and therefore were not concerned about local optima. An additional constraint was added that ~~requires~~ required the algorithm to cover South America before switching to North America to further prevent erratic scanning behavior. The pseudo-code ~~procedure of the~~ of the IO algorithm is shown in Algorithm 2.

3.6 ~~Evaluating the Optimized Scanning Strategy~~Parameter Exploration

~~To determine a "best" algorithm-selected scanning strategy, the global distribution of error, σ (Eq. (4)), of the algorithm-selected strategy is compared to a baseline scanning strategy that we considered the "obvious" choice if chosen by a human, shown in Fig. 5. We say the baseline strategy is the "obvious" choice because it tracks the sun's path and covers the entire area of interest in five coherent regions in the order of Tropical South America East, Tropical South America West, Temperate South America, Tropical North America, and Temperate North America. For scanning start and stop times of the baseline strategy, the same~~

Algorithm 2 Incremental Optimization Algorithm

$\mathbf{E} \leftarrow$ North American and South American land masses between $50^\circ N$ and $50^\circ S$

$\mathbf{S} \leftarrow$ Set of 5-minute east-to-west scan blocks where $E \subseteq \bigcup s_i \in \mathbf{S}$

$\mathbf{I} \leftarrow \emptyset$

$\mathbf{C} \leftarrow$ Objective Function

while $\mathbf{E} \subsetneq \mathbf{I}$ **do**

  Find $s^* \in \mathbf{S}$ such that $\mathbf{C}(s^*)$ is the minimum of the set $\{\mathbf{C}(s_i) : s_i \in \mathbf{S}\}$

  Append s^* to $\mathbf{I}$

  Remove s^* from $\mathbf{S}$

end while

~~times used by the IO algorithm are used for the baseline strategy (1230 UTC for the Autumn Equinox and 1315 UTC for the Summer Solstice).~~

3.7 ~~Parameter Exploration~~

~~In Equation~~ The IO algorithm calculates a scanning start time from a specified starting AF threshold, described in Sect. 3.2, but it was unknown what overall effect the AF threshold had on the overall performance of the resulting scanning strategy. In the objective function (Eq. (5)), the overlap and distance terms ~~have equal weighting in the objective function~~had equal weighting and different weightings were tested to understand their effects as well. A Monte Carlo experiment was performed to determine the distribution of sample error statistics across a range of possible starting AF thresholds and weights for overlap and distance. The effects of ~~weighting these~~ different weightings of the distance and overlap terms on the global distribution of errors were investigated specifically by adding (w_o, w_d) constant weight terms to Eq. (5) as new input parameters resulting in ~~Eq.~~

$$\mathrm{c}(s,t,w_o,w_d) = \psi(1 + \frac{w_o\phi + w_d\delta^2}{\beta}). \tag{6}$$

Applying Equation (6) ~~. Utilizing Equation 6, the algorithm now has three inputs~~ to the algorithm gives the operator three inputs to specify, w_o, w_d, and the starting ~~airmass factor threshold. A Monte Carlo experiment was performed to explore the parameter space of weights and determine the distribution of sample error statistics across the range of possible starting thresholds.~~ AF threshold. For both w_o and w_d, 1000 weights ~~each~~ were randomly sampled from a uniform distribution between 0 and 10. This process was repeated for the Summer Solstice and Autumn equinox for starting AF thresholds starting from 2.5 increasing by 0.1 to 3.5 ~~and found that the~~ for a total of 22,000 experiments. For these experiments, the contiguous land masses of North and South America were scanned with equal importance. The minimum variance of predicted errors ~~occurs when the~~ with respect to starting AF threshold ~~is~~ occured at 2.6 for the Summer Solstice and 2.7 for the Autumn Equinox , shown in Fig. 6. Both distributions of median and variance of errors averaged a 0.01 ppm spread over all values of w_o and w_d tested. Therefore, it was concluded that the effects of different weightings of the distance and overlap terms were negligible

on the overall aggregate error and weighting terms were excluded from the objective function. A sensitivity analysis was also done to quantify the effects of these results and can be found in Appendix A.

$$\mathrm{c}(s,t,w_o,w_d) = \mathrm{median}(e^{AF(s,t,x,y)}\alpha(x,y)^{-1})(1+\frac{w_o(s\cap\mathbb{I})+w_d\delta^2}{s\cap\mathbb{E}}).$$

4 ~~Results~~

3.1 ~~Global error~~

~~Based on the parameter exploration results , the global~~

3.1 Evaluating the Optimized Scanning Strategy

For evaluating the performance of an algorithm-selected scanning strategy, the empirical distributions of error~~were investigated for simulations during~~ , σ (Eq. (4)), were compared between the optimized strategy and a baseline scanning strategy proposed in Moore et al. (2018). An example of the two strategies are shown in Fig. 5. The baseline strategy tracks the sun's path from East to West and covers the entire area of interest in five coherent regions in the order of Tropical South America East, Tropical South America West, Temperate South America, Tropical North America, and Temperate North America. The same scanning start times used by the IO algorithm are used for evaluating the performance of the baseline strategy. The times are calculated by the algorithm, based on a starting AF threshold supplied by the user, were 1230 UTC for the Autumn Equinox with a starting AF threshold of 2.6 and 1315 UTC for the Summer Solstice with a starting AF threshold of 2.7.

In practice, a post-processing filter (PPF) is applied to retrieved satellite data and the data is marked with a quality flag to notify the end-user of its overall usefulness. For this study, a threshold of 100 on the SNR is used as our PPF to determine a "usable" sounding. This threshold limits the predicted error to a maximum of $\sim$ 2 ppm, (Eq. (4)), and is within the accuracy per sample performance requirements laid out in Polonsky et al. (2014).

4 Experiment 1 – Equal importance for all land masses

In the first experiment, all contiguous land masses of North and South America were scanned with equal importance. Based on the parameter exploration results, simulations were performed for the Summer Solstice with a starting AF threshold of 2.6 and ~~simulations during~~ the Autumn Equinox with a starting AF threshold of 2.7. The algorithm-selected scanning strategies consistently matched or exceeded the performance of the baseline scanning pattern, shown in ~~Fig~~Figs. 8 and 9. The region where the most significant improvement is seen is in the Amazon during the Autumn Equinox, refer to Fig. 10. ~~Additionally, the potential of both scanning strategies to yield observations where the SNR was greater than 100 (yielding a predicted error of $\sigma = 2.17$) was analyzed for both strategies~~After applying the PPF to the simulation results, it was clear that the greatest performance increase from the baseline strategy was in usable soundings. During the Summer Solstice, the algorithm-selected

strategy yielded ~~approximately~~ ~3.79 million usable soundings versus ~~the baseline strategy, which yielded approximately~~ ~3.02 million usable ~~soundings. Similarly during~~ from soundings the baseline strategy. During the Autumn Equinox, the algorithm-selected strategy yielded ~~approximately~~ ~4.31 million usable soundings versus ~3.04 million usable soundings from the baseline.

Part of the increase in usable soundings can be attributed to the optimized strategy following the coastline better, which results in less scans over the ocean and more overlapping scans, refer to Fig 5. However, the comparison of SZA and AF between the baseline and algorithm-chosen strategy shows that the algorithm also selects more scan blocks with low SZA and low AF, refer to Fig (11). It is important to note that these figures are ~~within~~ results from simulations done in the cloud-free environment of ~~our modeland~~ the model. Realistically, there is a high probability that parts of the scanning slit will include cloudy scenes, we expect the yield of usable soundings to be significantly less during operations, but ~~that will likely affect~~ those effects will be seen similarly in both the baseline and ~~optimal strategies similarly~~optimized strategies.

5 Experiment 2 – City campaign

A major advantage of having a geostationary platform is the flexibility to scan areas of high interest at times of optimal observing conditions. In this section, a "temporary campaign" mode is demonstrated where GeoCarb observes the ten most populous cities in North and South America as areas of high interest, which are New York, Chicago, Los Angeles, Dallas Fort-Worth, Mexico City, Bogota, Sao Paolo, Rio de Janeiro, Lima, and Buenos Aires. The demonstration is done for the Autumn Equinox with a starting AF threshold of 2.7. The areas of interest are given higher weighting in the algorithm through a modified version of Eq. (5). The performance of the resulting optimized strategies are compared to the baseline strategy, both globally and for the ten cities of interest.

5.1 ~~Sensitivity Analysis~~Modified Objective Function

To give these areas of interest a higher weight, a time-dependent scaling factor was added to the term ψ in the objective function (Eq. (5)) for scan blocks containing these cities, refer to Fig. 12. The scaling factor is defined as, e^{b-c}, where b is the AF of a point with respect to time and $c = a + e^{2-a}$, where a is the daily minimum AF of the point. The term c acts as a threshold for the selection of the scanning block. While b is greater than c, the scaling factor penalizes the objective function by giving it a larger value, which tells the algorithm to wait on selecting the block until it is reasonably close to its minimum AF. Once b becomes less than c, the scaling factor scales down the value of the objective function to make the algorithm select the scan block as soon as possible. Figure 13 shows the scaling factor for a point with a minimum daily AF of 2. Table 1 shows the relationship between minimum daily AF and the scaling factor threshold for a sample of minimum AFs. The modified objective function is

$$c(s,t) = \tilde{\psi}(1 + \frac{\phi + \delta^2}{\beta}), \tag{7}$$

where $\tilde{\psi}$ is the median of $e^{b-c}e^{AF}\alpha^{-1}$ over the entire area of a candidate scan block containing a city of interest.

5.2 Predicted errors

The addition of the scaling factor only affects the candidate scan blocks that contain a city of interest. Hence, there should be no significant degradation in the overall performance of the optimized scanning strategy. Fig. 14 shows that there is still a significant increase in usable soundings, ~ 3.97 million versus $\sim 3.03 million$ globally.

Looking at only observations over the ten cities, the optimized scanning strategy shows an increase of ~ 2000 usable soundings over the baseline strategy, refer to Fig. 15. Shown in Fig. 16, the baseline strategy's city observations have a higher concentration of low SZA soundings, but the optimized strategy's city observations have a higher concentration of low AF soundings.

6 Conclusions

We illustrate an efficient, offline technique that creates a geostationary scanning strategy that minimizes overall predicted measurement error. Applied in a simplified instrument model of GeoCarb, the IO routine gives us an optimized scanning strategy that performs better than the baseline scanning strategy relative to the global distribution of error and number of usable soundings. In Section 4, we showed that the incremental optimization of SNR with respect to the stationary physical processes, AF and albedo, results in an overall performance increase with the region of greatest performance increase seen in the Amazon (Fig. 9). We have also shown in Sect. 5 that the IO routine can be easily modified for a temporary campaign mode that focuses on the ten most populated cities of North and South America. Other examples of possible scenarios for temporary campaigns are wildfires, droughts, and volcanic eruptions.

At the moment, our model does not take into account the effect of clouds on retrieval quality. It is known that clouds play a significant role in scattering effects and influences τ in the calculation of radiance (Eq. (1)), but quantifying these effects is an active area of research. In a case study including clouds and aerosols in the atmosphere performed by Polonsky et al. (2014), the authors found that the number of usable soundings passing their post-processing filter (PPF) of aerosol optical depth (AOD) < 0.1 was between 8.1% to 20% of total simulated soundings. We believe that an AOD threshold of 0.1 is too strict for the clear sky atmosphere used in our simulations, therefore the threshold was relaxed to 0.3 to capture a conservative estimate of usable soundings as previously done by O'Dell et al. (2012) and Rayner et al. (2014). O'Dell et al. (2012) found that 22% of their simulated observations were classified correctly as "clear" when they used an AOD threshold of 0.3. Because we set $\tau = 0.3$ in our calculation of radiance (Eq. (1)), our estimate is that the true number of usable soundings will be around 20% of our simulated usable soundings in Sect. 4. Going forward, the incorporation of cloud products from CALIPSO will be investigated to better simulate operational conditions and produce more robust estimates of usable soundings.

The SNR-optimized scanning strategy outperforms the proposed strategy for the GeoCarb scientific observation plan. An empirical model that calculates predicted CO_2 retrieval uncertainty, σ, as a function of SNR was used to evaluate the performance of algorithm-selected strategies. The optimized scanning strategies consistently matched or exceeded the predicted

performance of the proposed scanning strategy pattern with respect to aggregate distribution of σ. When a simple post-processing filter (PPF) of SNR > 100 was applied to determine what constituted a usable sounding, the optimized strategies yielded a $\sim 18\%$ increase of usable soundings during the Summer and a $\sim 41\%$ increase during the Autumn over the proposed scanning strategy.

Data availability. The MCD43C3 MODIS BRDF/Albedo data was retrieved from the online Data Pool, courtesy of the NASA EOSDIS Land Processes Distributed Active Archive Center (LP DAAC), USGS/Earth Resources Observation and Science (EROS) Center, Sioux Falls, South Dakota, https://lpdaac.usgs.gov/.

Appendix A: Sensitivity Analysis

To quantify the algorithm's sensitivity to input parameters, the method of standardized regression coefficients (SRC) was utilized (Helton et al. (2006)). SRCs are the regression coefficients of a linear model fitted to the standardized dependent variable, $Y_Z = \frac{Y-\bar{Y}}{\sigma_Y}$, using standardized independent variables, $X_Z = \frac{X-\bar{X}}{\sigma_X}$. The dependent variable in this case is the predicted error and the independent variables are w_o, w_d, and the starting AF threshold. The standardization of variables allows for measuring the effect of the input parameters without their dependency on units (i.e. ~~km^2~~, ppm). The coefficient of determination, R^2, of the SRC model tells us how much of the variability in the sample statistics is explained by the SRC model. R^2 is defined as the Modeled Sum of Squares (MSS) divided by the Total Sum of Squares (TSS), where

$$\text{MSS} = \sum_{i=1}^{n} (\hat{Y}_i - \bar{Y})^2$$

$$\text{TSS} = \sum_{i=1}^{n} (Y_i - \bar{Y})^2$$

$$R^2 = \frac{\text{MSS}}{\text{TSS}}$$

and ~~$\hat{Y}$ = model predicted values, $\bar{Y}$ = mean Error, Y = observed values, n = number of observations.~~ $\hat{Y}$ = model predicted values, $\bar{Y}$ = r

The method of SRC was chosen for the sensitivity analysis by convenience of readily available simulation data from the parameter exploration experiment.

~~In the results,~~ The SRCs show that both the median and variance of the global error are found to be sensitive to starting AF thresholds as seen in ~~Fig~~Figs. 6 and 7, and Tables ~~1 and 2. The starting AF thresholds affect the scanning strategy as a whole by shifting the scanning time frame~~2 and 3. This sensitivity was expected considering that airmass factors ~~rely~~ depend on time and play a large role in the calculation of radiance (Eq. (1)). The starting AF thresholds affect the scanning strategy as a whole by shifting the scanning time frame. Because SRCs determine the effect of the input parameters in the presence of others, the SRCs fitted to a linear model of predicted error with respect to w_o and w_d were also analyzed within the Monte Carlo samples of starting AF threshold equal to 2.7 for the Autumn Equinox and starting AF threshold equal to 2.6 for the Summer Solstice.

Within the specified starting AF threshold of 2.7 for the Autumn Equinox, moderate effects of the weights were found on the sample global error distribution. The values in Table ~~3~~ 4 show that the SRC model explains approximately half of the variability in median of global error distributions, $R^2 = 0.552$, and the parameter with the largest effect on the variance is the distance, δ. With respect to variance of global error distributions, the SRC model explains less than half of the variability with $R^2 = 0.384$. Again, the parameter with the largest effect is the distance term.

Within the specified starting AF threshold of 2.6 for the Summer Solstice, the effects of the weights on the sample global error distribution are small. The SRC model explains ~~approximately~~ around a quarter of the variability in median of global error distributions, $R^2 = 0.242$, and ~~approximately 15%~~ $\sim 15\%$ of the variability with $R^2 = 0.148$, shown in Table ~~4.~~ 5. The parameter with the largest effect is the overlap term for both variance and median of error distributions.

~~Small~~ R^2 values ~~signify little~~ less than 0.7 signify small sensitivity to the independent variables or a nonlinear relationship between the independent and dependent variables. Visual analysis of the scatter plots of the distributions of sample statistics versus weights (Fig. A1) does not imply a nonlinear relationship between the weights and sample statistics.

~~We illustrate an efficient technique that selects a covering set that also minimizes global measurement error. The Incremental Optimization routine gives us an optimized scanning strategy that performs better than the baseline scanning strategy relative to the global distribution of error and number of usable soundings. We also found that by optimizing for the global distribution of error, we obtained an improvement in regional errors~~ It is important to note as well, ~~seen in Fig. 9. There may be better objective functions to optimize, and the structure of the algorithm does allow human intervention beyond the scope of this work. For example, in the event of natural phenomena such as wildfires, droughts, and volcanic eruptions, the algorithm can be modified to capture prioritized scanning regions during the minimum predicted error time for those regions.~~ that the non-standardized sensitivity of predicted errors with respect to w_o, w_d results in a spread of 0.01 ppm in the overall performance of an algorithm-selected scanning strategy. We conclude that the weighting terms contribute negligible effects to the algorithm's performance.

~~At the moment, our model does not take into account the effect of clouds on retrieval quality. It is known that clouds play a significant role in scattering effects and influences the calculation of radiance (Eq. (1)). In a case study by Polonsky et al. (2014) that included clouds and aerosols in the atmosphere, they found that the number of usable soundings passing their post-processing filter (PPF) of AOD < 0.1 was between 8.1% to 20% of total simulated soundings. We believe that an AOD threshold of 0.1 is too conservative for a clear sky AOD threshold, therefore it was relaxed to 0.3 as previously done by Rayner et al. (2014) and O'Dell et al. (2012). In O'Dell et al. (2012), they found that 22% of scenes were classified correctly as "clear" when they used an AOD threshold of 0.3. Because $\tau = 0.3$ in our calculation of radiance (Eq. (1)), we estimate that the true number of usable soundings will be around 20% of our original estimates of daily usable soundings in Sect. 4.1. Going forward, cloud products from CALIPSO will be incorporated to better simulate operational conditions. This will yield more robust scanning strategies and estimates of usable soundings.~~

~~The SNR-Optimized scanning strategyoutperforms the human-selected strategy first proposed for the GeoCarb scientific observation plan. The algorithm selects strategies that consistently match or exceed the performance of the baseline scanning~~

~~pattern with respect to global error. The algorithm-selected strategies yield an 18% increase of soundings with a SNR>100 during the Summer and a 41% increase during the Autumn over the baseline strategy.~~

Author contributions. SC conceptualized the goals of this project. JN and SC developed the methodology together. BM provided oversight and guidance. JN prepared the manuscript, developed the algorithm code, model code, and executed the simulations.

Competing interests. The authors report no competing interests.

Acknowledgements. Some of the computing for this project was performed at the OU Supercomputing Center for Education & Research (OSCER) at the University of Oklahoma (OU). This work was supported by NASA award No. 80LARC17C0001.

References

Crisp, D., Atlas, R., Breon, F.-M., Brown, L., Burrows, J., Ciais, P., Connor, B., Doney, S., Fung, I., Jacob, D., Miller, C., O'Brien, D., Pawson, S., Randerson, J., Rayner, P., Salawitch, R., Sander, S., Sen, B., Stephens, G., Tans, P., Toon, G., Wennberg, P., Wofsy, S., Yung, Y., Kuang, Z., Chudasama, B., Sprague, G., Weiss, B., Pollock, R., Kenyon, D., and Schroll, S.: The Orbiting Carbon Observatory (OCO) mission, Advances in Space Research, 34, 700–709, https://doi.org/10.1016/J.ASR.2003.08.062, 2004.

Crisp, D., Miller, C. E., and DeCola, P. L.: NASA Orbiting Carbon Observatory: measuring the column averaged carbon dioxide mole fraction from space, Journal of Applied Remote Sensing, 2, 023 508, https://doi.org/10.1117/1.2898457, 2008.

Crisp, D., Pollock, H. R., Rosenberg, R., Chapsky, L., Lee, R. A. M., Oyafuso, F. A., Frankenberg, C., O'Dell, C. W., Bruegge, C. J., Doran, G. B., Eldering, A., Fisher, B. M., Fu, D., Gunson, M. R., Mandrake, L., Osterman, G. B., Schwandner, F. M., Sun, K., Taylor, T. E., Wennberg, P. O., and Wunch, D.: The on-orbit performance of the Orbiting Carbon Observatory-2 (OCO-2) instrument and its radiometrically calibrated products, Atmospheric Measurement Techniques, 10, 59–81, https://doi.org/10.5194/amt-10-59-2017, 2017.

Eldering, A., O'Dell, C. W., Wennberg, P. O., Crisp, D., Gunson, M. R., Viatte, C., Avis, C., Braverman, A., Castano, R., Chang, A., Chapsky, L., Cheng, C., Connor, B., Dang, L., Doran, G., Fisher, B., Frankenberg, C., Fu, D., Granat, R., Hobbs, J., Lee, R. A. M., Mandrake, L., McDuffie, J., Miller, C. E., Myers, V., Natraj, V., O'Brien, D., Osterman, G. B., Oyafuso, F., Payne, V. H., Pollock, H. R., Polonsky, I., Roehl, C. M., Rosenberg, R., Schwandner, F., Smyth, M., Tang, V., Taylor, T. E., To, C., Wunch, D., and Yoshimizu, J.: The Orbiting Carbon Observatory-2: first 18 months of science data products, Atmospheric Measurement Techniques, 10, 549–563, https://doi.org/10.5194/amt-10-549-2017, 2017a.

Eldering, A., Wennberg, P. O., Crisp, D., Schimel, D. S., Gunson, M. R., Chatterjee, A., Liu, J., Schwandner, F. M., Sun, Y., O'Dell, C. W., Frankenberg, C., Taylor, T., Fisher, B., Osterman, G. B., Wunch, D., Hakkarainen, J., Tamminen, J., and Weir, B.: The Orbiting Carbon Observatory-2 early science investigations of regional carbon dioxide fluxes, Science, 358, eaam5745, https://doi.org/10.1126/science.aam5745, 2017b.

Gloor, M., Fan, S.-M., Pacala, S., and Sarmiento, J.: Optimal sampling of the atmosphere for purpose of inverse modeling: A model study, Global Biogeochemical Cycles, 14, 407–428, https://doi.org/10.1029/1999GB900052, 2000.

Hammerling, D. M., Michalak, A. M., O'Dell, C., and Kawa, S. R.: Global CO ₂ distributions over land from the Greenhouse Gases Observing Satellite (GOSAT), Geophysical Research Letters, 39, https://doi.org/10.1029/2012GL051203, 2012.

Helton, J. C., Johnson, J. D., Sallaberry, C. J., and Storlie, C. B.: Survey of sampling-based methods for uncertainty and sensitivity analysis, Reliability Engineering and System Safety, 91, 1175–1209, https://doi.org/10.1016/j.ress.2005.11.017, 2006.

Hetland, M. L.: Greed Is Good? Prove It!, pp. 139–161, Apress, Berkeley, CA, https://doi.org/10.1007/978-1-4842-0055-1_7, 2014.

Karp, R. M.: Reducibility among Combinatorial Problems, pp. 85–103, Springer US, Boston, MA, https://doi.org/10.1007/978-1-4684-2001-2_9, 1972.

Kumer, J. J. B., Rairden, R. L., Roche, A. E., Chevallier, F., Rayner, P. J., and Moore, B.: Progress in development of Tropospheric Infrared Mapping Spectrometers (TIMS): GeoCARB Greenhouse Gas (GHG) application, Proc.SPIE, 8867, 8867 – 8867 – 16, https://doi.org/10.1117/12.2022668, 2013.

Kuze, A., Suto, H., Nakajima, M., and Hamazaki, T.: Thermal and near infrared sensor for carbon observation Fourier-transform spectrometer on the Greenhouse Gases Observing Satellite for greenhouse gases monitoring, Appl. Opt., 48, 6716–6733, https://doi.org/10.1364/AO.48.006716, 2009.

Lucht, W., Schaaf, C. B., and Strahler, A. H.: An algorithm for the retrieval of albedo from space using semiempirical BRDF models, IEEE Transactions on Geoscience and Remote Sensing, 38, 977–998, https://doi.org/10.1109/36.841980, 2000.

Miller, C. E., Crisp, D., DeCola, P. L., Olsen, S. C., Randerson, J. T., Michalak, A. M., Alkhaled, A., Rayner, P., Jacob, D. J., Suntharalingam, P., Jones, D. B. A., Denning, A. S., Nicholls, M. E., Doney, S. C., Pawson, S., Boesch, H., Connor, B. J., Fung, I. Y., O'Brien, D., Salawitch, R. J., Sander, S. P., Sen, B., Tans, P., Toon, G. C., Wennberg, P. O., Wofsy, S. C., Yung, Y. L., and Law, R. M.: Precision requirements for space-based data, Journal of Geophysical Research: Atmospheres, 112, https://doi.org/10.1029/2006JD007659, 2007.

Moore, B., Crowell, S. M. R., Rayner, P. J., Kumer, J., O'Dell, C. W., O'Brien, D., Utembe, S., Polonsky, I., Schimel, D., and Lemen, J.: The Potential of the Geostationary Carbon Cycle Observatory (GeoCarb) to Provide Multi-scale Constraints on the Carbon Cycle in the Americas, Frontiers in Environmental Science, 6, 1–13, https://doi.org/10.3389/fenvs.2018.00109, 2018.

Nickless, A., Rayner, P. J., Erni, B., and Scholes, R. J.: Comparison of the genetic algorithm and incremental optimisation routines for a Bayesian inverse modelling based network design, Inverse Problems, 34, 055 006, 2018.

O'Brien, D. M., Polonsky, I. N., Utembe, S. R., and Rayner, P. J.: Potential of a geostationary geoCARB mission to estimate surface emissions of CO_2, CH_4 and CO in a polluted urban environment: case study Shanghai, Atmospheric Measurement Techniques, 9, 4633–4654, https://doi.org/10.5194/amt-9-4633-2016, 2016.

O'Dell, C. W., Connor, B., Bösch, H., O'Brien, D., Frankenberg, C., Castano, R., Christi, M., Eldering, D., Fisher, B., Gunson, M., McDuffie, J., Miller, C. E., Natraj, V., Oyafuso, F., Polonsky, I., Smyth, M., Taylor, T., Toon, G. C., Wennberg, P. O., and Wunch, D.: The ACOS CO2retrieval algorithm-Part 1: Description and validation against synthetic observations, Atmospheric Measurement Techniques, 5, 99–121, https://doi.org/10.5194/amt-5-99-2012, 2012.

Patra, P. K. and Maksyutov, S.: Incremental approach to the optimal network design for CO2 surface source inversion, Geophysical Research Letters, 29, 971–974, https://doi.org/10.1029/2001GL013943, 2002.

Polonsky, I. N., O'Brien, D. M., Kumer, J. B., O'Dell, C. W., and the geoCARB Team: Performance of a geostationary mission, geoCARB, to measure CO_2, CH_4 and CO column-averaged concentrations, Atmospheric Measurement Techniques, 7, 959–981, https://doi.org/10.5194/amt-7-959-2014, 2014.

Rayner, P. J., Enting, I. G., and Trudinger, C. M.: Optimizing the CO2 observing network for constraining sources and sinks, Tellus B, 48, 433–444, https://doi.org/10.1034/j.1600-0889.1996.t01-3-00003.x, 1996.

Rayner, P. J., Utembe, S. R., and Crowell, S.: Constraining regional greenhouse gas emissions using geostationary concentration measurements: a theoretical study, Atmospheric Measurement Techniques, 7, 3285–3293, https://doi.org/10.5194/amt-7-3285-2014, 2014.

Schaaf, C. and Wang, Z.: MCD43C3 MODIS/Terra+Aqua BRDF/Albedo Albedo Daily L3 Global 0.05Deg CMG V006 [Data set], https://doi.org/10.5067/MODIS/MCD43C3.006, 2015.

Yokota, T., Yoshida, Y., Eguchi, N., Ota, Y., Tanaka, T., Watanabe, H., and Maksyutov, S.: Global Concentrations of CO2 and CH4 Retrieved from GOSAT: First Preliminary Results, SOLA, 5, 160–163, https://doi.org/10.2151/sola.2009-041, 2009.

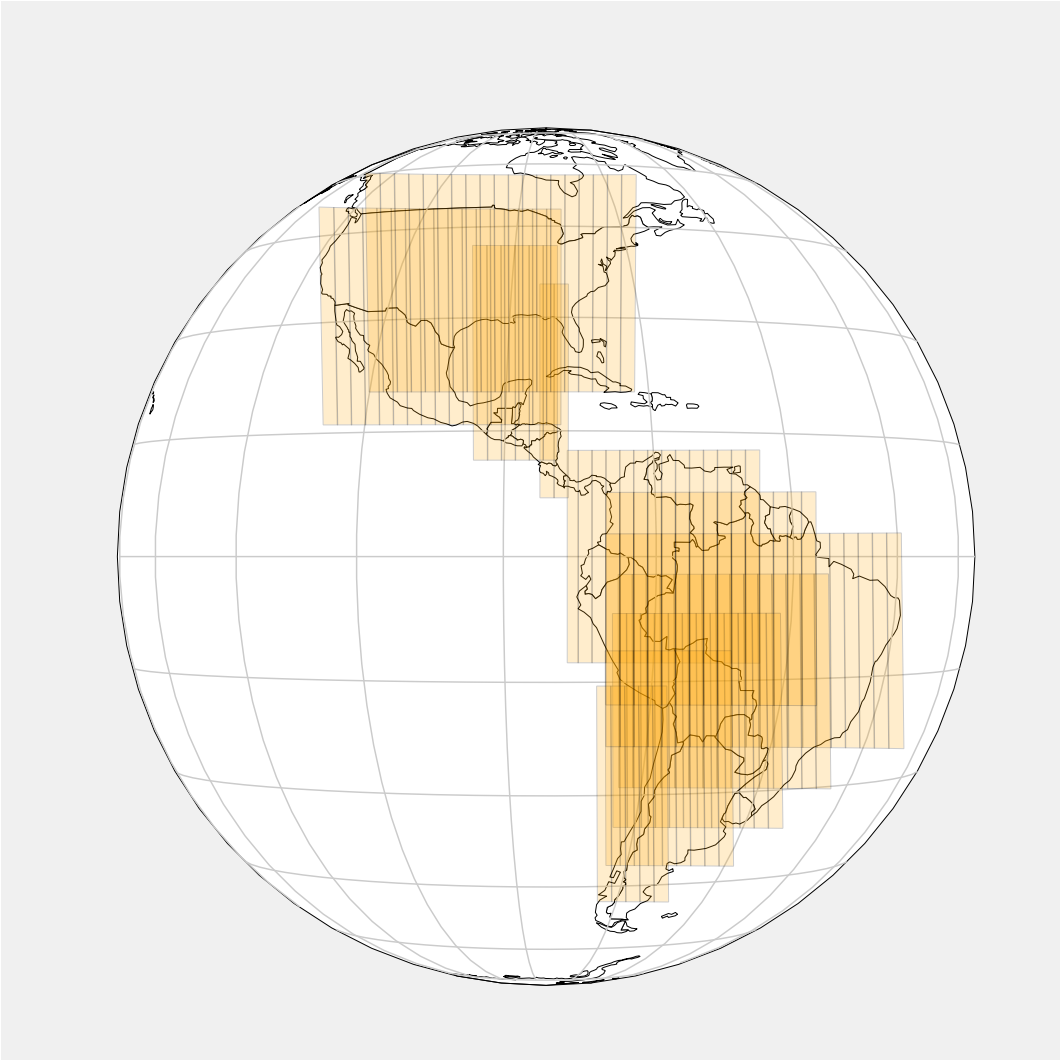

Figure 1. Candidate Scan Blocks.

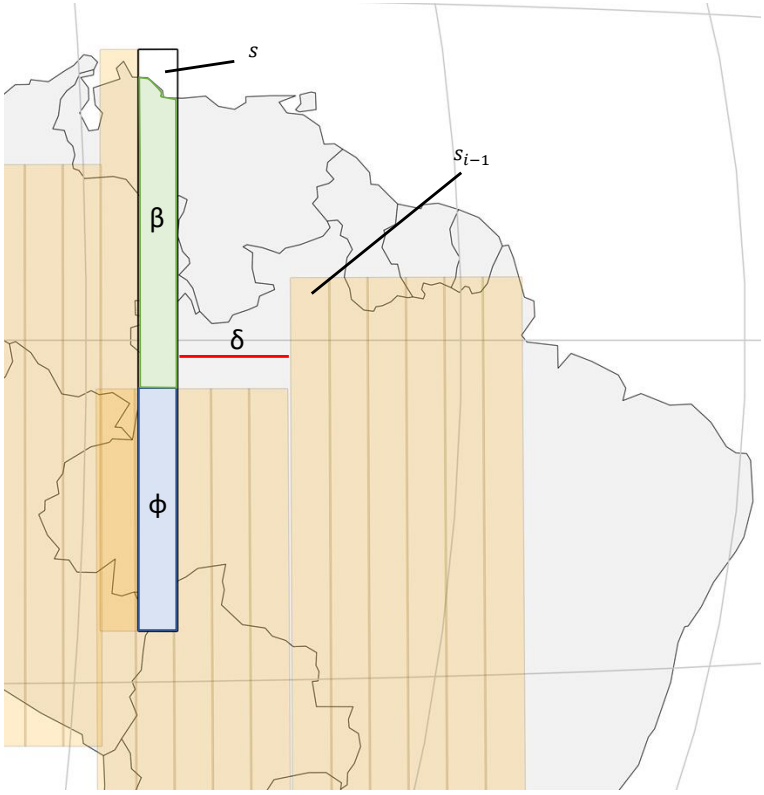

Figure 2. A diagram explaining the objective function, c(s,t), used in the IO routine. The block labeled, s_{i-1}, is the last selected block and the block labeled, s, is the block for which c(s,t) is being calculated.

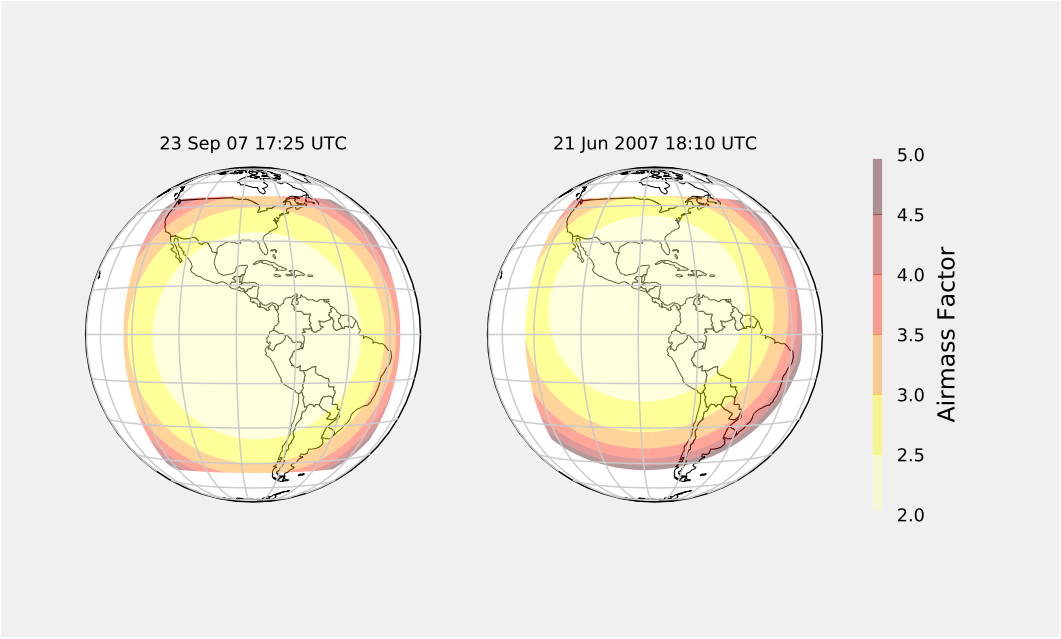

Figure 3. Comparing airmass factors in ~~June~~ September (left) and ~~December~~ June (right).

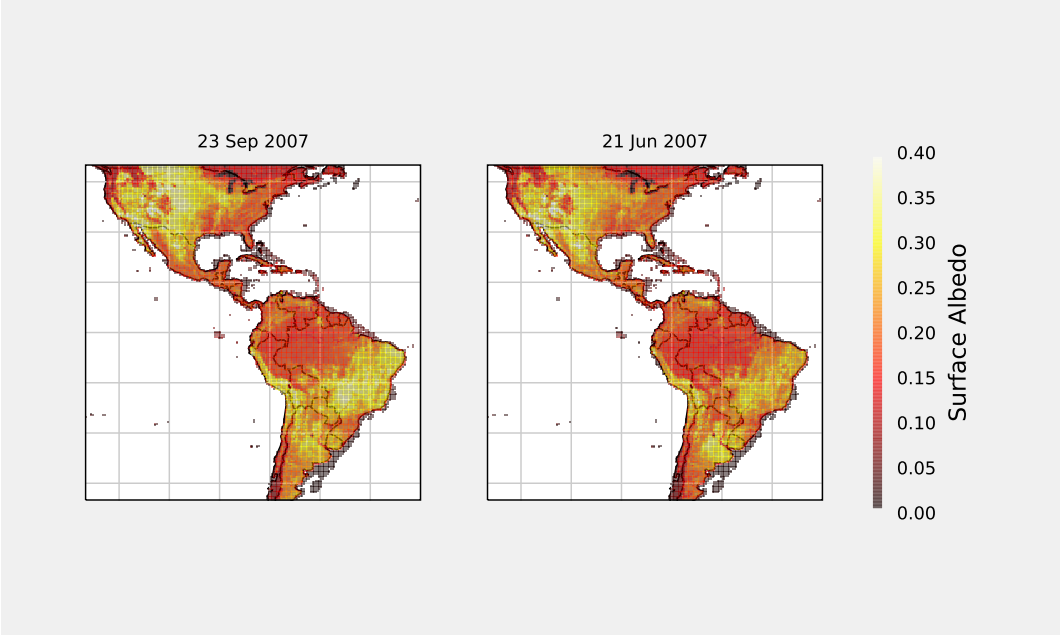

Figure 4. Comparing Surface Albedo during the Autumn Equinox (left) and the Summer Solstice (right).

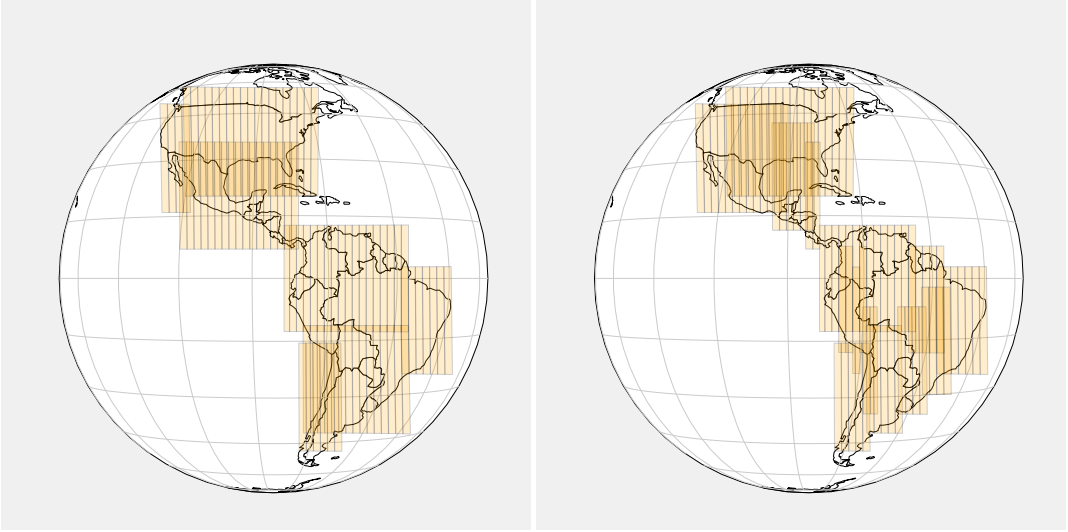

Figure 5. The ~~"obvious" choice~~ baseline strategy (left) compared to an algorithm-selected strategy (right).

a	c	$c - a$
2.0	3.0	1
2.3	3.041	.741
2.5	3.107	.607
2.7	3.197	.497
3.0	3.36	.36
4.0	4.135	.135
4.95	5.0	.05

Table 1. This table shows for a sample of daily minimum AFs the distance relationship between the daily minimum AF of an observed point, a, and the scaling factor threshold, c, used in the modified objective function (Eq. (7)).

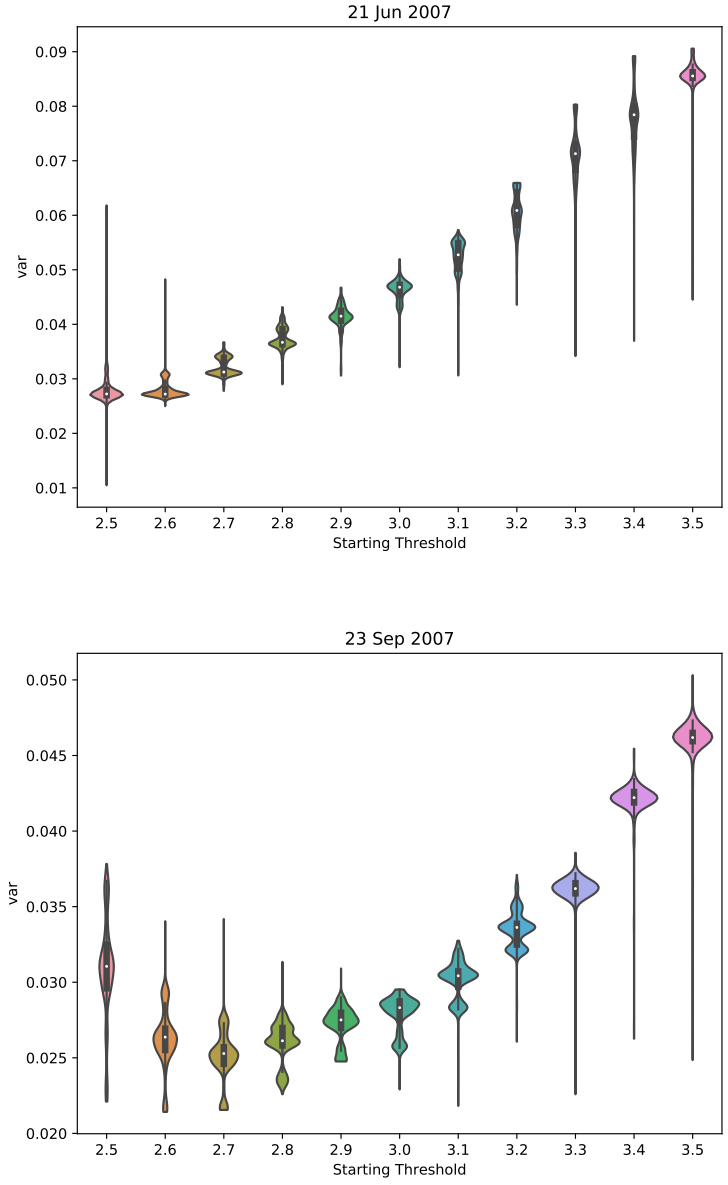

Figure 6. Violin plots show the effect of starting threshold on variance of errors: Summer Solstice (top) and Autumn Equinox (bottom).

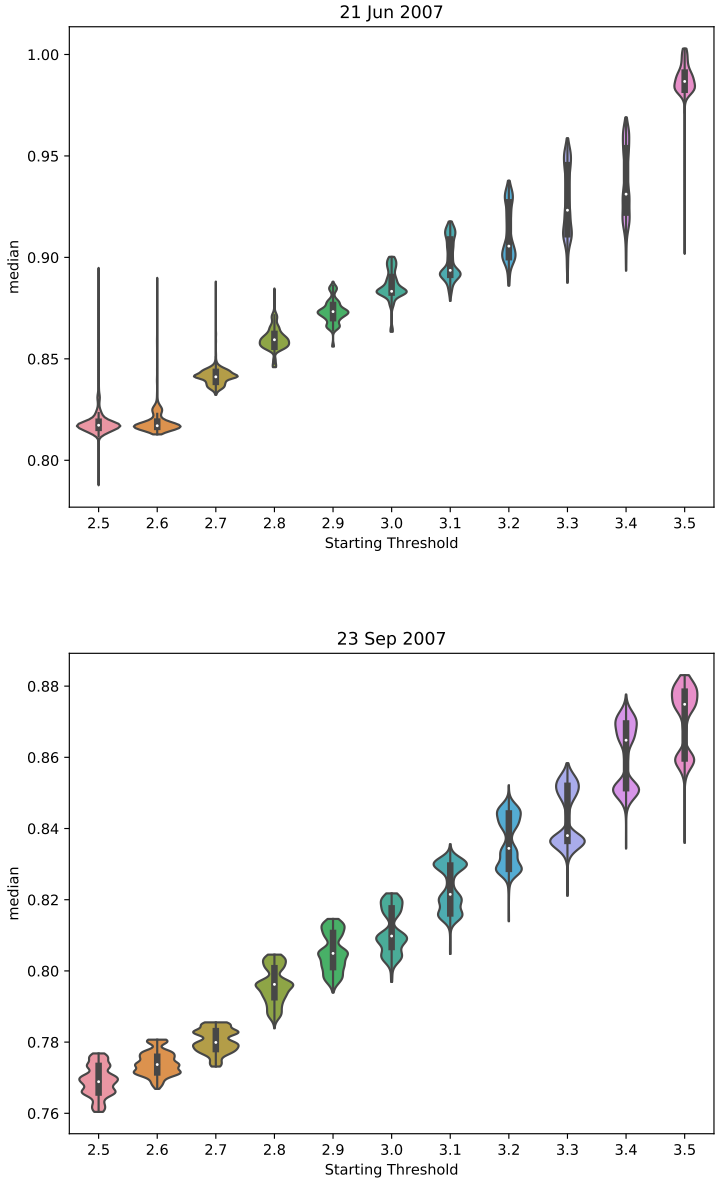

Figure 7. Violin plots show the effect of starting threshold on error distribution medians: Summer Solstice (top) and Autumn Equinox (bottom).

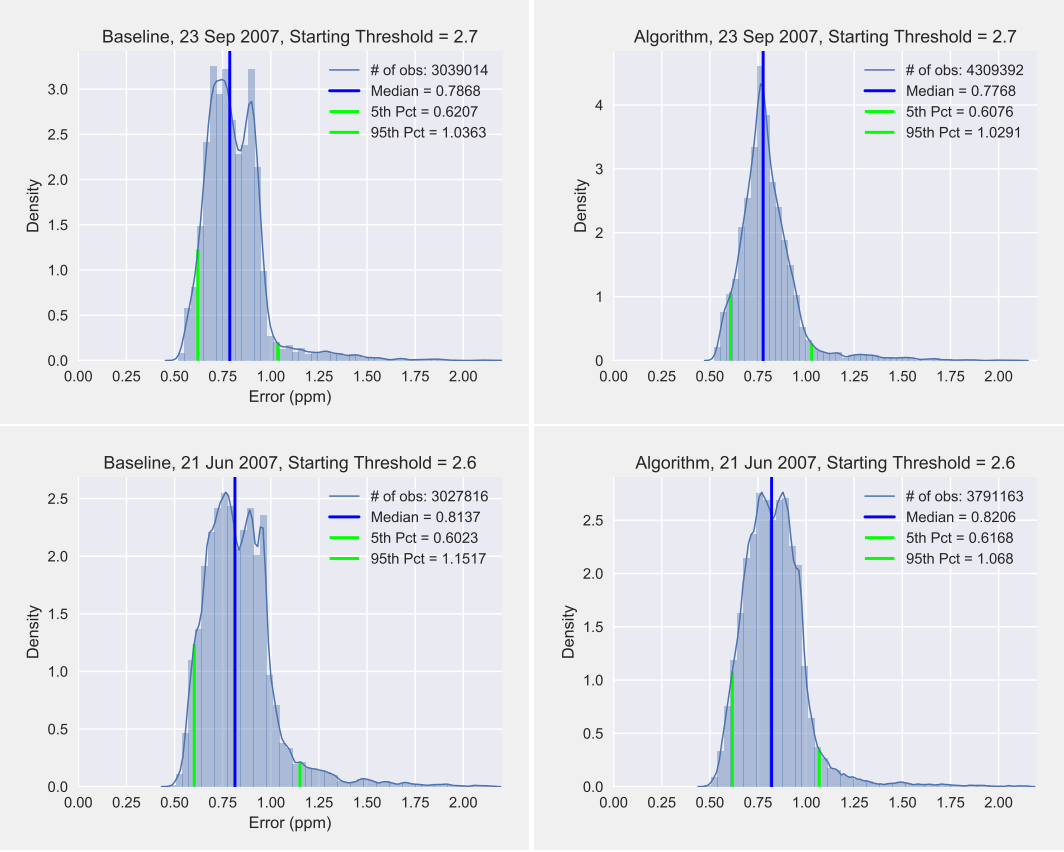

Figure 8. Global error distribution, baseline strategy (left) and algorithm-selected strategy (right).

Standardized Regression Coefficients, Summer Solstice			
Input Parameters	Variance	Median	Expected Usable Observations
R^2	0.939	0.935	0.311
Starting Threshold	0.9679	0.9618	-0.2769
w_o	0.0615	-0.0621	-0.0634
w_d	-0.0040	-0.0716	0.4839

Table 2. The SRCs show that the variance and median of global error distributions are sensitive to starting AF thresholds.

~~The SRCs show that the starting AF threshold has major effect on variance and median of global error distributions.~~

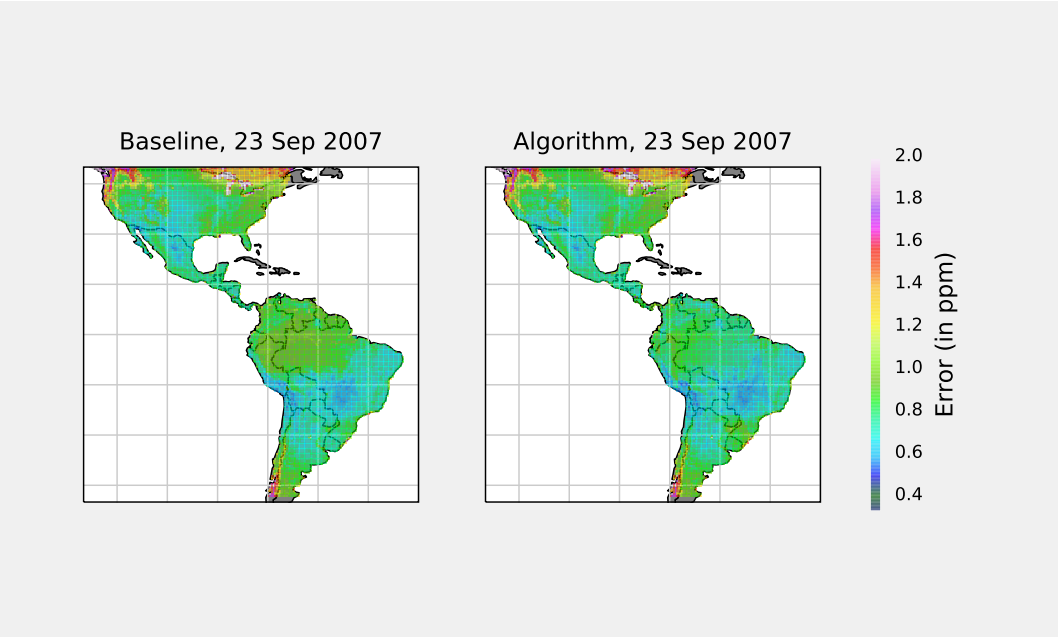

Figure 9. Comparing the algorithm-selected strategy (right) to the baseline strategy (left).

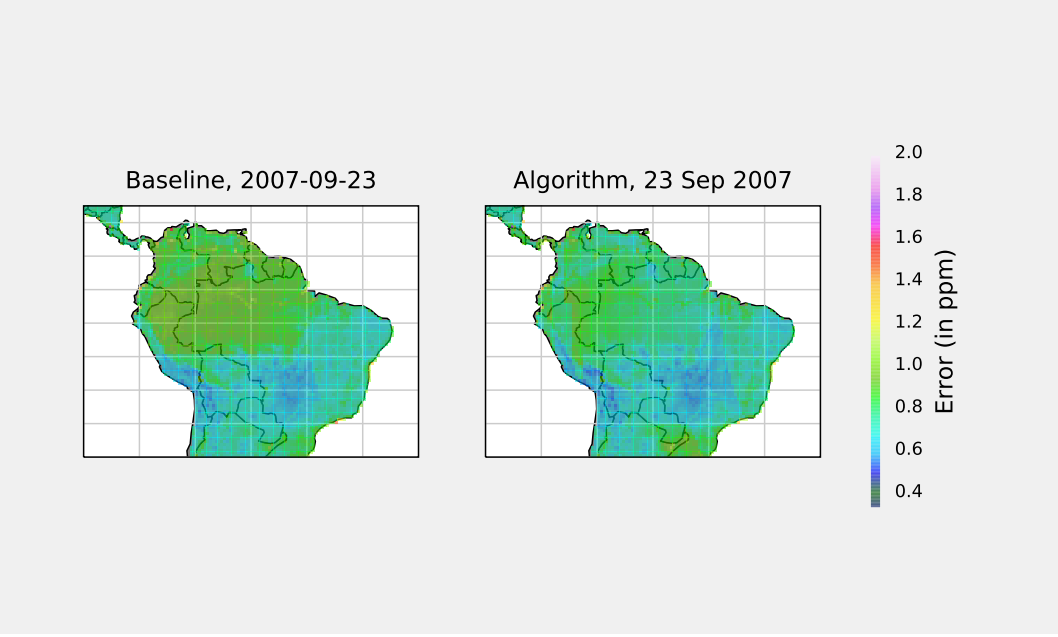

Figure 10. There is a significant improvement in predicted errors over the Amazon for the Autumn Equinox.

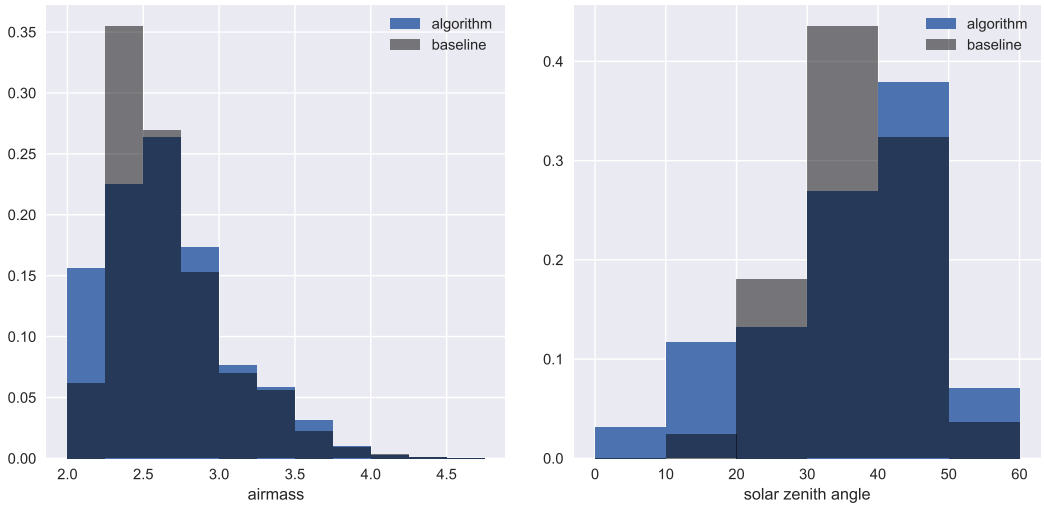

Figure 11. The histograms show that the algorithm selects more scan blocks with low AF (left) and low SZA (right) than the baseline strategy.

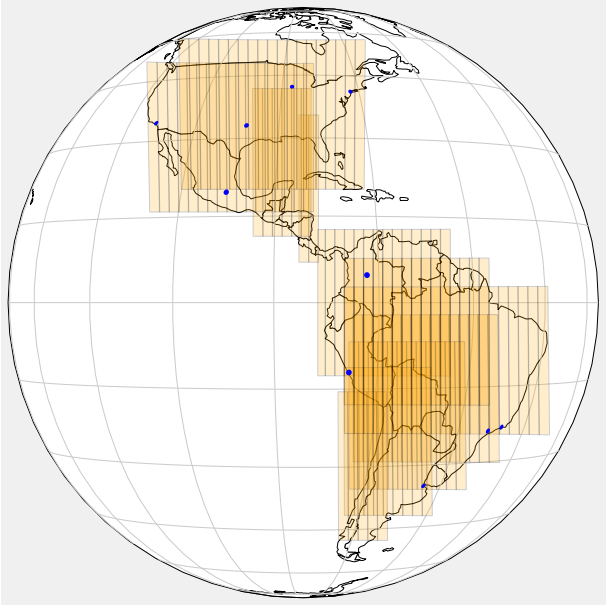

Figure 12. Scan blocks containing the ten most populated cities are given higher weighting in city campaign mode.

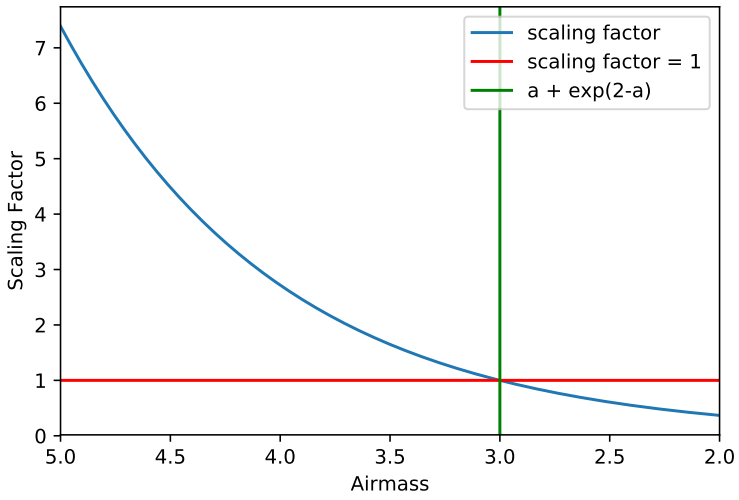

Figure 13. Scaling Factor for an observation point with minimum daily airmass factor, $a = 2$.

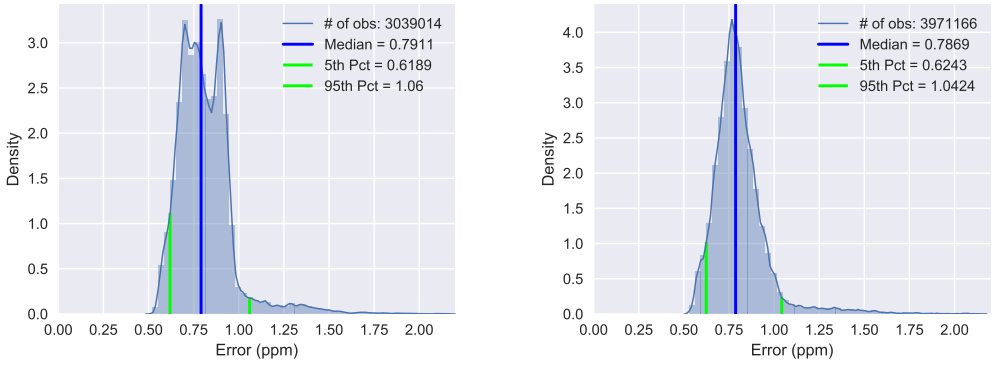

Figure 14. Compared to the baseline strategy (left), the overall performance of the algorithm-selected strategy (right) is not significantly degraded in the city campaign mode.

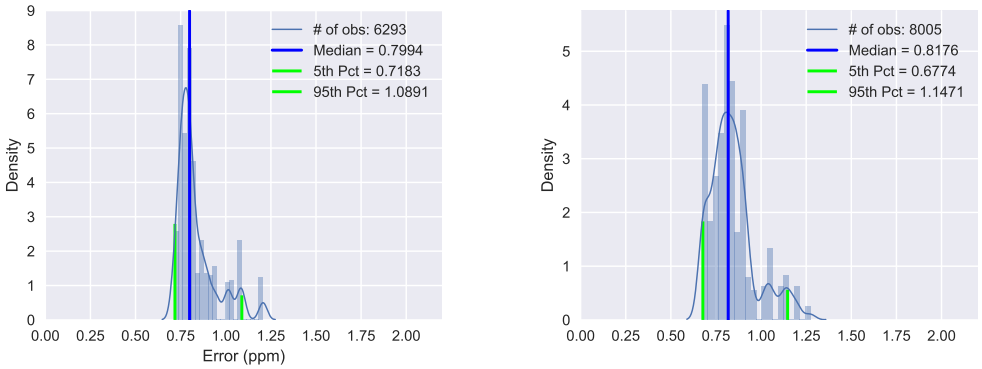

Figure 15. Compared to the baseline strategy (left), the algorithm-selected strategy in city campaign mode (right) sees an increase of approx. 2000 usable soundings over the ten most populated cities.

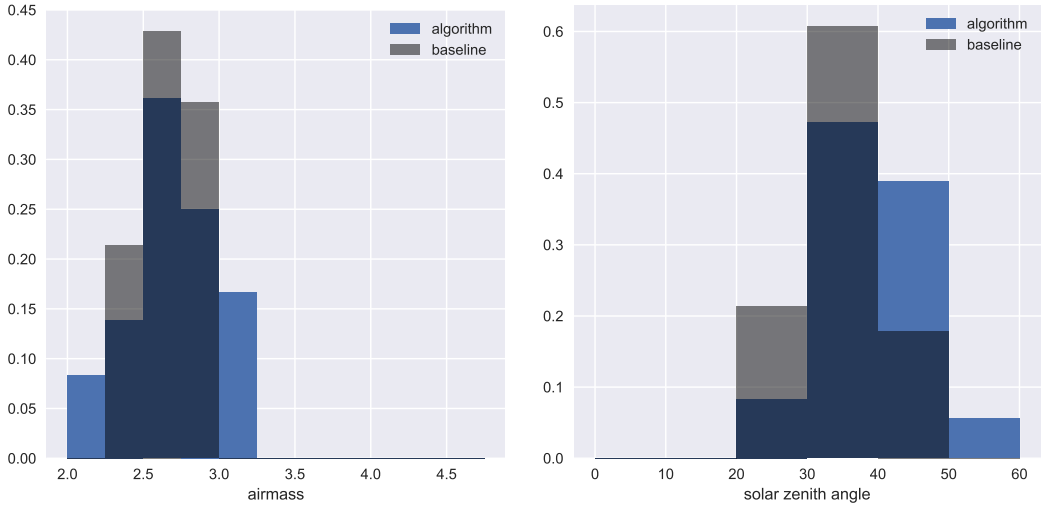

Figure 16. In the city campaign mode, the histograms show that the algorithm-selected strategy has more observations with low AF (left), but the baseline strategy's observations have lower SZA (right).

Standardized Regression Coefficients, Autumn Equinox			
Input Parameters	Variance	Median	Expected Usable Observations
R^2	0.646	0.977	0.208
Starting Threshold	0.7997	0.9770	-0.4473
w_o	-0.0163	0.0056	-0.0579
w_d	0.0757	0.1455	0.0772

Table 3. The SRCs show that the median of global error distributions is sensitive to starting AF thresholds. The low R^2 value for variance indicates that there may be a nonlinear relationship between variance and starting AF threshold. Fig. 6 shows that this is the case.

~~The SRCs show that the starting AF threshold has major effect on median and variance of global error distributions~~

SRC for Starting Threshold = 2.7, Autumn Equinox			
Input Parameters	Variance	Median	Expected Usable Observations
R^2	0.384	0.552	0.497
w_o	-0.3051	0.2502	-0.2310
w_d	0.5450	0.6950	0.6702

Table 4. The SRCs show that the median and variance of global error distributions are not senstive to different weighting of the distance and overlap terms. $R^2 < 0.7$ usually signifies insensitivity to independent variables.

~~The SRCs show that the distance term has a moderate effect on the median of global error distributions and some effect on variance of global error distributions during the Autumn Equinox.~~

SRC for Starting Threshold = 2.6, Summer Solstice			
Input Parameters	Variance	Median	Expected Usable Observations
R^2	0.148	0.242	0.284
w_o	-0.3481	-0.4833	-0.3911
w_d	-0.1717	-0.1064	0.3519

Table 5. The SRCs show that the median and variance of global error distributions are not senstive to different weighting of the distance and overlap terms. $R^2 < 0.7$ usually signifies insensitivity to independent variables.

~~The coefficients of determination tell us that the weighting has little effect on global error distribution during the Summer Solstice.~~

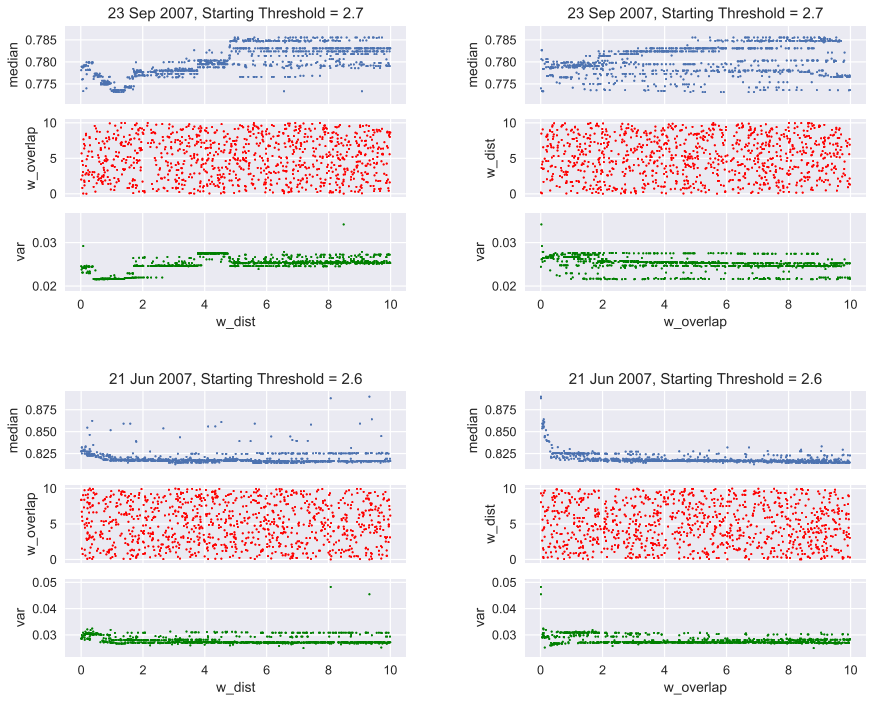

Figure A1. Scatter plots do not indicate a nonlinear relationship between weights and sample statistics. w_o and w_d are indicted as w_dist and w_overlap in the x-axis.